Measuring Acoustic Mobility of Particles by Particle Tracking Velocimetry

Alexander Edthofer
2022
Masters' Thesis in Biomedical Engineering

Supervisor: Dr Thierry Baasch, Dr. Andreas Lenshof
Examiner: Dr. Wei Qui

LUND
UNIVERSITY

Faculty of Engineering LTH
Department of Biomedical Engineering

Abstract

Acoustophoresis is a method to manipulate and move cells or particles suspended in a medium using acoustic waves. The speed of the acoustophoretic motion depends on the cells' acoustic mobility, i.e. their size, density and compressibility relative to the medium. Differences in acoustic mobility can be used to separate particles from each other. Separation is an important tool within biomedical and clinical applications.
In this thesis, we develop a method to measure the acoustic mobility of a particle or cell with Particle Tracking Velocimetry (PTV) software. The acoustic mobility determines the migration velocity, thus it is possible to determine the acoustic mobility by measuring the migration velocity.
As several particles' acoustic mobilities are determined, they can be used to assess optimal buffer conditions to maximise the relative acoustic mobility between two particles or cells, improving their separation by acoustophoresis.
In this thesis, a simple rectangular microfluidic chip was filled with particles suspended in a solution. The migration of particles due to exposure to an acoustic standing wave field was then repeatedly imaged and the procedure was repeated 20 times collect sufficient data. The particle paths and migration velocities can be extracted by PTV software. By fitting this velocity to a theoretical model the acoustic mobility can be derived.
The experimental set-up and computational model were already present at the Thomas Laurell group at BMC, Lund University where this thesis was conducted. They were, however, lacking sufficient precision and reliability, yielding a wide spread of data points for each experiment and resulting in large variations in measurements between experiments. Thus, the main focus of this thesis primarily revolved around improving the experimental procedures, data processing and the computational model. The long-term goal of this project is to create an easy to use, reliable and rapid method to determine the acoustic properties of any given cell and propose a suitable medium composition for ideal separation.

One improvement of the model is the division of the images into thinner slices to achieve more local and accurate measurements. Another change was the intro-

duction of a velocity filter, excluding data that stemmed from particles with only minimal movement unrelated to the migration effects induced by the acoustic field. The thesis also improved and evaluated the experimental set-up in itself, focusing on the usage of fluorescent Polystyrene beads as reference particles as well as evaluating the accuracy of the model and detecting errors in it. This resulted in the discovery of significant differences in the acoustic properties of differently coloured polystyrene particles which were confirmed by an independent experiment.
Finally, the experimental model was used in preliminary measurements of three different breast cancer cell lines' acoustic mobility.

Acknowledgements

I would like to thank my supervisors, Thierry Baasch and Andreas Lenshof, for always coming with ideas and possible solutions for the countless of issues, weird results and not working matlab - code that made up most of this thesis.
Special thanks to Thomas Laurell for inspiring me to apply for this thesis and nurturing my interest in acoustophoresis en large and of course for accepting my application for this master thesis.
Additionally, I would like to thank Cecilia Magnusson, Klara Andersson , Megan Havers, Axel Broman, Eva Undvall for helping me out in the laboratory, having weird discussions over fika and being great co-workers in general. Special thanks to Simon Olsson and Linda Péroux, for co-operating in several experiments and sharing much of this experience (and sometimes frustrations) with me and always being down to discuss and complain about our various issues with experiments.
I want to thank Fredrik Dunge, Andre Rath, Axel Helgstrand and Linda Péroux for being the most ridiculous group of friends I could possibly imagine and turning my Saturday afternoons into fantastical and hilarious adventures. (Just remember to never split the party, guys).

Nomenclature

Symbol	Description	Unit
a	Radius	m
ASD	Average standard deviation	
BAW	Bulk acoustic waves	
c_0	Speed of sound	m/s
c_1	Amplitude fitting coefficient	
c_2	Wavenumber fitting coefficient	
d	Distance	m
DLD	Deterministic lateral displacement	
E_{ac}	Time-average acoustic energy density	N/m^2
f_1	Monopole scattering coefficient	
f_2	Dipole scattering coefficient	
$\boldsymbol{F}_{\text{drag}}$	Stokes drag force	N
$\boldsymbol{F}_{\text{g}}$	Gravitational force	N
$\boldsymbol{F}_{\text{inertial}}$	Inertial force	N
$\boldsymbol{F}_{\text{rad}}$	Acoustic radiation force	N
$\boldsymbol{F}_{\text{viscous}}$	Viscous force	N
FACS	Fluorescence-activated cell sorting	
Hz	Hertz	s^{-1}
k	Wavenumber	m^{-1}
p-wave	Primary wave	
PTV	Particle Tracking Velocimetry	
POM	Polyoxymetylene	
SAW	Surface acoustic waves	
SD	Standard deviation	
PZT	Lead Zirconite Titanite	
R_{N}	Reynolds number	
$\mathbf{v}$	Velocity	m/s
V_{pp}	Peak-to-peak voltage	$\text{kgm}^2\text{s}^{-3}\text{A}^{-1}$

Symbol	Description	Unit
Γ	Viscous correction factor of $\boldsymbol{F}_{\text{rad}}$	
δ	Viscous boundary layer thickness	m
Δx	Difference in x-direction	m
η	Dynamic viscosity	$\text{kgm}^{-1}\text{s}^{-1}$
κ	Compressibility	m^2/N
λ	Wavelength	m
π	Pi	
ρ	Mass density	kg/m^3
σ	Poisson's ratio	
Φ	Acoustic contrast factor	
χ	Hydrodynamic correction factor of $\boldsymbol{F}_{\text{drag}}$	
ω	Angular frequency	rads^{-1}

Contents

List of Figures

List of Tables

1

Introduction

1.1 Project Outline and Motivation

The ability to quickly and easily separate different cells is of great interest in medical and biotechnological research. For example, being able to sort cells into distinct populations is necessary to study individual cell types isolated from a heterogeneous starting population. [**1**]
One method to do this is acoustophoresis, which employs the force that originates from the scattering interaction between particles and sound waves to move the cells in a medium. This force depends on the acoustic mobility, the product of particle size and their contrast factor. The contrast factor is a function of the particles' density and mobility relative to the surrounding medium. As different particles will have a different acoustic mobility, they move at different speeds in the medium, which allows separation.

This thesis aims to develop and evaluate a method to measure the acoustic mobility. This is done by a combined numerical and experimental approach, where acoustophoresis causes particles to migrate and Particle Tracking Velocimetry (PTV) is used to track their migration. The method is part of a larger research development that aims at improving the efficacy and efficiency of particle separation methods using acoustophoresis.
An already completed set-up served as a starting point for the thesis, however, the accuracy and repeatability of measurements were not sufficient to determine the contrast factor of unknown particles. This was tackled by improving the data processing steps within MatLab and expanding the experimental protocol.

Polystyrene particles of varying sizes and fluorescent agents were evaluated with the set-up. This revealed significant differences in their contrast factors, which is interesting as they are common reference and calibration particles. These differences were confirmed by a separate experimental method. Furthermore, the acoustic mobility and contrast factor of melamine resin as well as three different breast cancer

cell lines, BT20; BT549 and MCF7, were measured.

2

Background and Theory

2.1 Chip Design

The microfluidic chip used for the measurement of acoustic properties of particles in this thesis is made of silicon and bonded anodically to a glass slide to allow the microscope and camera to observe the channel. It is 40.7 mm long, 3 mm wide and 1.67 mm high. A sketch of the chip can be seen in figure 2.1.

The microfluidic channel itself was etched into the silicon before the glass was bonded to it and is 375 μm wide, 150 μm high and 35.7 mm wide, with 1 mm wide holes on each end that serve as inlet and outlet respectively.

Two transducers made of lead zirconite titanate (PZT Pz26) are glued to the bottom of the chip using cyanoacrylate superglue, with the required wiring having been soldered unto the bottom of them.
The two transducers have different dimensions, as their resonance frequency depends on their thickness.[**2**] The thickness of the transducer, which is going to operate at around 5 MHz to create a horizontal node, is 0.4 mm, whilst the transducer creating the vertical node, operating at 2 MHz, is 1 mm thick.
To leave easy access for any tubing and wires, the chip is secured unto a holder with a hollowed-out section beneath the channel, as shown in figure 2.2.

2.2 Experimental Set-up

The particles are suspended in a buffer and loaded into a syringe. The buffer is pumped through the device by a syringe pump (2.3a) & 2.4a), SP210i Syringe Pump). To quickly be able to switch between flow and no flow, the fluid goes through a multiport valve (2.3b) & 2.4b)). Here, one mode leads the fluid through a hydrodynamic short circuit into the waste (2.3c) & 2.4c)), which is active when the flow inside the chip is stopped. The hydrodynamic short circuit prevents wobbling and backflow when switching between starting and stopping the flow through the

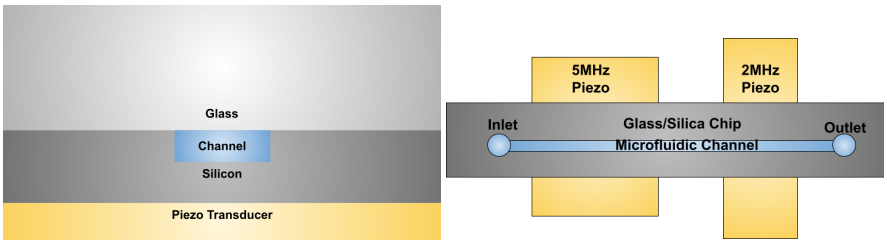

(a) Cross sectional view of the microfluidic device. (b) Top view of the microfluidic device.

Figure 2.1 The microfluidic device used in the measurement of particles' acoustic properties. It contains a simple, straight channel with an inlet and outlet. Two piezo-transducers are glued to the device.

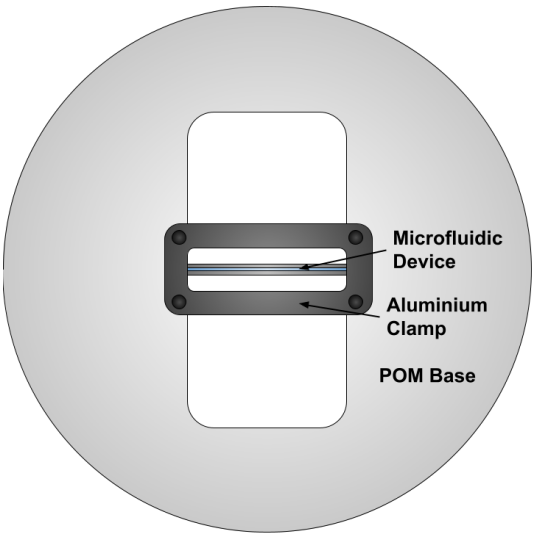

Figure 2.2 The holder is made with a Polyoxymetylene (POM) base, using CNC milling to make the details and screw sockets. The device was secured onto it using an aluminium clamp.

channel. The second mode leads the fluid through the chip device, which fills and flushes the device between measurements (2.3d) & 2.4d)).

The transducers (2.3e) & 2.4e)) attached to the chip are controlled by a function generator (2.3f) & 2.4f), Tektronix AFG3022C) and amplifiers (2.3g) & 2.4g)).
A second function generator (Tektronix AFG3022B) is used to externally control the camera framerate. The chip is imaged by a Leica DM 2500 microscope (2.3h)

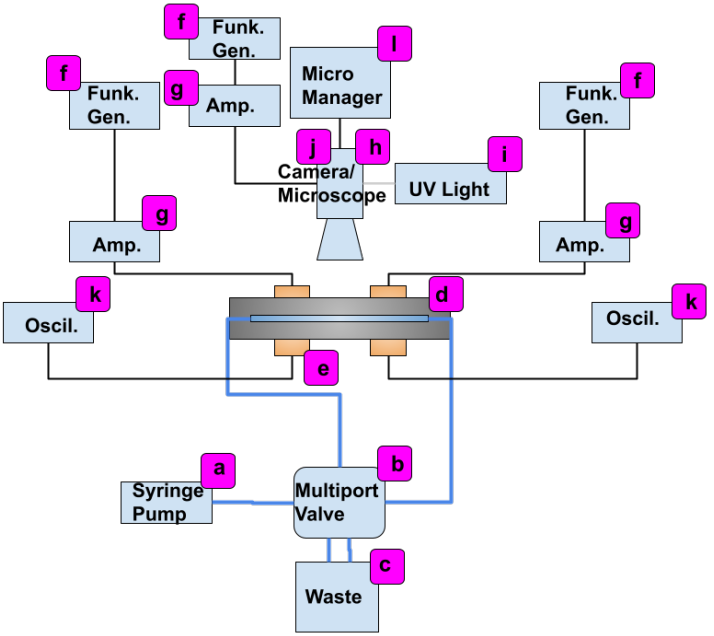

Figure 2.3 Sketch of the experimental set-up. a) Syringe pump. b) Multiport valve. c) Waste. d) Microfluidic chip. e) Piezo Transducer. f) Function Generators. g) Amplifiers. h) Microscope. i) Fluorescent light source. j) Camera. k) Oscilloscope. l) MicroManager2.0.

& 2.4h)) and a 20x/0.40 objective, with an X-Cite 120Q as light source for the TRITC and FITC modes (2.3i) & 2.4i)). The microscope is connected to an Andor Zyla scMos camera (2.3j) & 2.4j)), which is controlled by the Micro-Manager 2.0 program (2.3l) & 2.4l)) to image and record the channel. An oscilloscope (2.3k) & 2.4k)), Tektronix TDS 1002) measures the voltage in the piezotransducers.

2.3 Microfluidics

Laminar Flow

At the small scales and low velocities typically present in microsystems, the viscous forces dominate over the inertial forces and the non-linear terms of the Navier-Stoke's equation are expected to be negligible. To determine if this is the case for a given system, we can analyse the velocity fields' Reynolds number, a dimensionless parameter that is derived from the ratio of inertial and viscous forces,

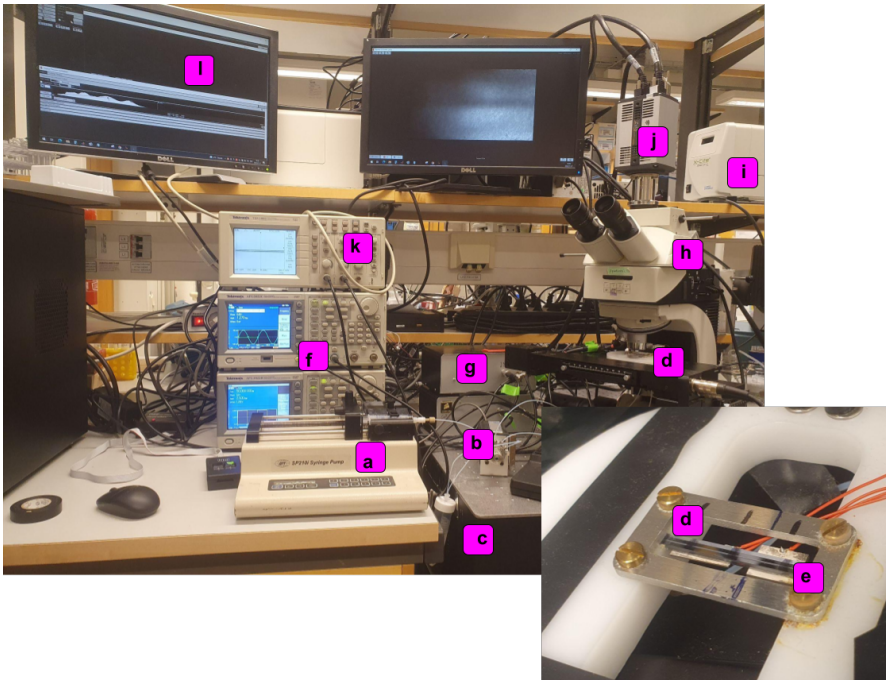

Figure 2.4 Experimental Set-up for the acoustic factor measurements. a) Syringe pump. b) Multiport valve. c) Waste. d) Microfluidic chip. e) Piezo Transducer. f) Function Generators. g) Amplifiers. h) Microscope. i) Fluorescent lightsource. j) Camera. k) Oscilloscope. l) MicroManager2.0 program

$$R_N = \frac{\boldsymbol{F}_{\text{inertial}}}{\boldsymbol{F}_{\text{viscous}}} = \frac{\rho \mathbf{v}_c d}{\eta}, \tag{2.1}$$

where ρ is the density, $\mathbf{v}_c$ the characteristic velocity, d the characteristic linear dimension (e.g. pipe diameter) and η the dynamic viscosity of the fluid. A Reynolds number below 2000 is generally considered to indicate a laminar flow, above 4000 is usually turbulent and between 2000 and 4000 is often in the critical regime.[**3**]

This laminar flow is the basic premise of microfluidics. In laminar flow mixing only occurs through diffusion, a far slower process than the mixing in turbulent flow. External forces become a potent tool to manipulate particles in laminar flow, as they can easily become the dominant influence on the particles' movement.
Such forces include shear force due to proximity to the walls of the channel, gravity, electromagnetic fields and acoustic fields.

Stokes drag

If an external force moves a cylindrical particle with radius a with a velocity $\mathbf{v}_p$ relative to the fluids velocity $\mathbf{v}_0$, the movement causes a drag force directed in the opposite direction of the movement of the particle through the fluid. This force is known as Stokes drag, $\boldsymbol{F}_{\text{drag}}$: [**4**]

$$\boldsymbol{F}_{\text{drag}} = 6\pi\eta a(\mathbf{v}_0 - \mathbf{v}_p). \tag{2.2}$$

In a microfluidic device, the channel walls of the device introduce a hydrodynamic drag. This issue was resolved by Faxén [**5**] by introducing a correction factor $\chi(a)$ to the drag force F_{drag}. For a gap with a distance h between two parallel plates and a particle with a radius a moving parallel to the wall, the correction factor is described by

$$\chi = [1 - 1.004(\frac{2a}{h}) + 0.418(\frac{2a}{h})^3]^{-1}. \tag{2.3}$$

This correction factor is then simply multiplied with the expression for the drag force, $\boldsymbol{F}_{\text{drag}}$:

$$\boldsymbol{F}_{\text{drag}} = -6\pi\eta a\mathbf{v}_p\chi(a). \tag{2.4}$$

For particle diameters <10μm and a channel width of 375μm the correction factor never exceeds 1.0565 and could thus be neglected for initial measurements. It might be worthwhile to take it into account when the measurement method becomes more accurate and larger cells and particles are measured.

2.4 Acoustophoresis

Acoustic Actuation

Acoustic waves can either be generated using Bulk Acoustic Waves (BAW), which is driven by a piezoelectric transducer attached to the microchip, or Surface Acoustic Waves (SAW), using an interdigitated transducer on a piezoelectric surface.[**6**; **7**] They greatly differ and have their respective advantages, but in this work we focus on BAW.

The piezo transducers in the thesis are driven by harmonic electric signals on the MHz scale, sending MHz vibration into the chip and its surroundings. By matching the half-wavelength with the width of the channel, the impedance mismatch between the medium and channel wall creates resonances that lead to standing acoustic waves with a central nodal plane in the middle of the channel.

This thesis uses two differently sized transducers, transmitting waves with different wavelengths to create standing waves in both the vertical and horizontal planes of the channel.

Acoustic Radiation Force

A spherical particle suspended in an acoustic field will act as a point scatterer, which causes some of the acoustic waves' momentum to be transferred to the particle.
The transfer of momentum is described with the time-averaged acoustic radiation force $\boldsymbol{F}_{\text{rad}}$, which was first proposed by Yosioka and Kawasima in 1955 [**8**] and later expanded by Bruus and Settnes [**9**]. For a one-dimensional acoustic standing wave creating a vertical nodal plane, as illustrated in figure 2.5, $\boldsymbol{F}_{\text{rad}}$ is found by

$$\boldsymbol{F}_{\text{rad}} = 4\pi\Phi a^3 k E_{\text{ac}} sin(2ky), \tag{2.5}$$

E_{ac} is the acoustic energy density, a the radius of the particle, k the wavenumber, y the position of the particle and Φ the contrast factor.

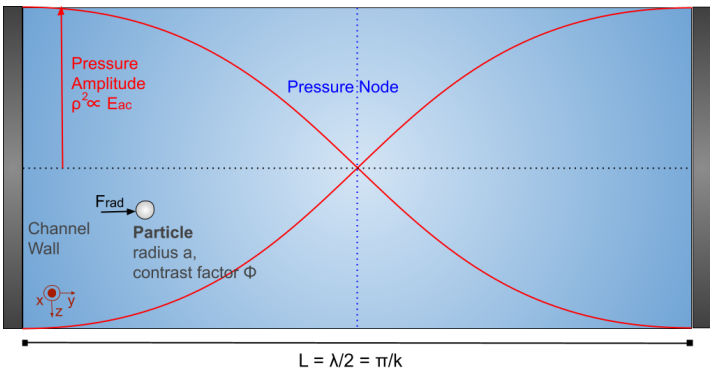

Figure 2.5 Illustration of the radiation force $\boldsymbol{F}_{\text{rad}}$ on a particle in a one-dimensional acoustic standing wave. For a positive Φ, the particle moves towards the pressure node.

Acoustic Streaming

A second-order effect that arises in acoustophoresis is the steady-state acoustic streaming due to the attenuation of acoustic waves.
In an acoustofluidic device, this effect is driven by bulk flow attenuation or by Schlichting and Rayleigh streaming.

The bulk flow can be ignored in this thesis, as we assume bubble-free solutions and operate at length scales smaller than the required attenuation length for bulk streaming.[**10**]

The viscous boundary induced acoustic streaming is a rotational motion known as Schlichting rolls. [**11**] These occur within the viscous boundary layer thickness

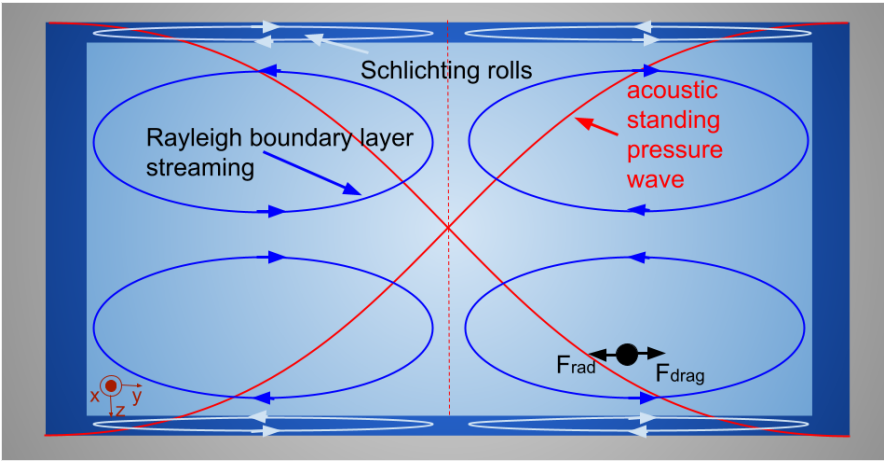

Figure 2.6 Sketch of the acoustic streaming inside of a microchannel (grey). The imposed acoustic standing wave (red) creates boundary layer streaming rolls (Schlichting rolls) inside of the thin boundary layer (intermediate blue), which drive acoustic streaming rolls in the bulk fluid (Rayleigh streaming). A particle (black) in this system is subject to an acoustic radiation force and drag force.

$\delta = \sqrt{\frac{2\nu}{\omega}}$, with ν being the sound velocity speed and $\omega = 2\pi f$ the angular frequency.

Both the Rayleigh streaming [**12**] and Schlichting rolls are illustrated in figure 2.6. The derivation of the force on a particle due to boundary layer acoustic streaming is beyond the scope of this thesis and is negligibly for particles significantly larger than the boundary layer thickness. [**13**]

Negligible Forces

As particles come close to each other, they influence each other through hydrodynamic or acoustic particle-particle interactions. This is shown experimentally in this thesis, as particle solutions with increasing particle concentrations were measured. For simplicity, we want to neglect those interaction forces in our measurements. The effect can be neglected for a sufficiently dilute solution, such that the particle distances $\gg 4a$, as the hydrodynamic forces are negligible above this threshold. [**14**]

Due to particles' small volume and similar density to the surrounding medium, the gravitational force $\boldsymbol{F}_g$ is negligible for the short time periods during which particles are tracked. [**15**]

2.5 Movement of Particles in an Acoustic Field

To derive a functioning theoretical model for the measurement of particles' acoustic mobility, we look at how a single particle moves in a 1D acoustic standing wave due to the forces introduced in the previous section.

If the size of a particle is above a critical size a_c [**16**] the movement of a particle is dominated by the acoustic radiation force $\boldsymbol{F}_{\text{rad}}$, causing it to migrate towards the so called minimum Gorkov potential. This potential minimum is located at the pressure node for particles with a positive Φ and at the anti-pressure node for particles with a negative Φ. [**17**]
This movement through the fluid is resisted by the viscous drag force, $\boldsymbol{F}_{\text{drag}}$.

The total force on the particle, $\boldsymbol{F}_{\text{tot}}$, illustrated in figure 2.7, is the sum of them:

$$F_{\text{tot}} = F_{\text{rad}} + F_{\text{drag}} = 4\pi\Phi a^3 k E_{\text{ac}} sin(2ky) - 6\pi\eta a \mathbf{v}_{\text{p}}(y). \tag{2.6}$$

At dynamic equilibrium $\boldsymbol{F}_{\text{tot}} = 0$, which gives us:

$$4\pi\Phi a^3 k E_{\text{ac}} sin(2ky) = 6\pi\eta a \mathbf{v}_{\text{p}}(y). \tag{2.7}$$

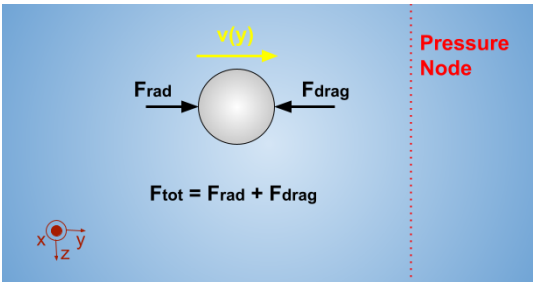

Figure 2.7 The movement of the particle towards the pressure node due to $\boldsymbol{F}_{\text{rad}}$ is opposed to $\boldsymbol{F}_{\text{drag}}$. At dynamic equilibrium, the sum of forces is 0.

In the experimental part of this thesis, we measure the velocity of the particle, thus the equation is rewritten to isolate $\mathbf{v}_{\text{p}}(y)$:

$$\mathbf{v}_{\text{p}}(y) = -\frac{2}{3}\frac{\Phi a^2 k E_{\text{ac}}}{\eta} sin(2ky). \tag{2.8}$$

2.6 Numerical Model

As part of the numerical model in this thesis, the velocity and position of a particle along the y-dimension is fitted to a sinusoidal curve by the least squares method.

This fitting generates three constants, c_1, c_2 and c_3. c_1 describes the amplitude of the fitted curve, c_2 describes the wave number and c_3 describes the phase shift of the sinusoidal curve. Thus, the sinusoidal curve can be describes as

$$\mathbf{v}(y) = c_1 sin(c_2 y) + c_3. \tag{2.9}$$

Comparing equation 2.12 and 2.13, c_1 can be described as

$$c_1 = -\frac{2}{3}\frac{\Phi a^2 k E_{\text{ac}}}{\eta} \tag{2.10}$$

and c_2 as

$$c_2 = 2k. \tag{2.11}$$

Combining these equations gives

$$c_1 = -\frac{1}{3}\frac{\Phi a^2 c_2 E_{\text{ac}}}{\eta}. \tag{2.12}$$

Depending on whether Φ or E_{ac} is unknown, the equation can be rewritten and solved:

$$E_{\text{ac}} = -3\frac{\eta c_1}{\Phi a^2 c_2} \tag{2.13}$$

$$\Phi a^2 = -3\frac{\eta c_1}{E_{\text{ac}} c_2}. \tag{2.14}$$

With this equation it is possible to measure the acoustic mobility of any given particle with a known radius as long as the properties of the channel and acoustic field are known. By measuring different particles under the same experimental conditions, it is therefor possible to calculate the ratio of their acoustic mobilities:

$$\Phi_{p1} a_{p1}^2 = -3\frac{\eta c_{1;p1}}{E_{\text{ac}} c_{2;p1}}. \tag{2.15}$$

$$\Phi_{p2} a_{p2}^2 = -3\frac{\eta c_{1;p2}}{E_{\text{ac}} c_{2;p2}}. \tag{2.16}$$

$$\frac{\Phi_{p1} a_{p1}^2}{\Phi_{p2} a_{p2}^2} = \frac{-3\frac{\eta c_{1;p1}}{E_{\text{ac}} c_{2;p1}}}{-3\frac{\eta c_{1;p2}}{E_{\text{ac}} c_{2;p2}}} = \frac{c_{1;p1} c_{2;p2}}{c_{1;p2} c_{2;p1}} \tag{2.17}$$

The size of a particle can be measured by numerous different approaches. The size of the polystyrene beads used in this thesis was measured with a Coulter counter, as it has the advantage of giving the full distribution.[**18**]
The size of breast cancer cells was measured by ImageStream flow cytometry, as the Coulter counter was broken.

To calculate the energy density, the contrast factor experiment is first performed with a reference particle with known acoustic properties, such as polystyrene beads.

In this thesis, 5.18 μm green fluorescent polystyrene beads (microParticles GmbH, Germany), were used as reference particles. The contrast factor is calculated with the relation between the particles and the mediums density and compressibility:

$$\Phi = \frac{1}{3} f_1(\bar{\kappa}) + \frac{1}{2} f_2(\bar{\rho}) \tag{2.18}$$

$$f_1(\bar{\kappa}) = 1 - \bar{\kappa}; \bar{\kappa} = \frac{\kappa_p}{\kappa_0} \tag{2.19}$$

$$f_2(\bar{\rho}) = \frac{2\bar{\rho} - 2}{2\bar{\rho} + 1}; \bar{\rho} = \frac{\rho_p}{\rho_0}. \tag{2.20}$$

The density ρ_p of polystyrene beads is 1050 kg/m^3. [**19**] The compressibility is calculate with: [**20**]

$$\kappa_p = \frac{3(1-\sigma_p)}{1+\sigma_p} \frac{1}{\rho_p c_p^2}, \tag{2.21}$$

where σ_p = 0.35 [**21**] is the Poisson's ratio and c_p = 2350 m/s [**22**] is the p-wave speed through polystyrene.
This gives $\kappa_p = 249\text{TPa}^{-1}$.

In all measurements on non-organic particles such as polystyrene beads, melamine resin and silicon beads, Milli-Q water with a density ρ_0 = 1000 kg/m^3 [**19**] and a speed of sound c_0 = 1500 m/s [**19**] is used, which gives a compressibility $\kappa_0 = 448\text{TPa}^{-1}$. Note that Poisson's ratio can be neglected for fluids.

This gives a calculated contrast factor

$$\Phi_{\text{PS}} = \frac{1}{3} f_1(\bar{\kappa}) + \frac{1}{2} f_2(\bar{\rho}) = 0.165 \tag{2.22}$$

for polystyrene beads suspended in Milli-Q water.

As Φ_{PS} is used for all reference calibrations performed in this thesis, we briefly compare our calculated value to other works.
Baasch et. al. had assumed Φ_{PS} to be 0.1619 as provided by the manufacturer of the polystyrene particles in 2018. [**15**] In Hartonos work on cell compressibility, a Φ_{PS} of 0.526 was used. [**23**]. Another paper from 2010, by Barnkob, found Φ_{PS} to be 0.328. [**24**] A later paper by Barnkob from 2012 however found Φ_{PS} to be 0.17. [**25**]. From this brief review, we can conclude that the most recent papers stating

Φ_{PS} find similar values as we have calculated in this thesis.

To control if the acoustic radiation force is dominating over the streaming forces for these polystyrene particles, we calculate the critical radius a_c:

$$a_c = \sqrt{\frac{3\Psi}{2\Phi}}\delta, \tag{2.23}$$

where Ψ is a geometry-dependent factor, with $\Psi = 3/8$ for a standing wave parallel to a planar wall.[**16**]
The viscous boundary layer thickness δ is calculated assuming a frequency of 2MHz in Milli-Q, which gives: $\delta = 0.38\mu$m.
This gives us

$$a_c = \sqrt{\frac{\frac{9}{8}}{2 \cdot 0.165} \cdot 0.38 \cdot 10^{-6}} = 1.14\mu\text{m}, \tag{2.24}$$

which is a significantly smaller radius than the polystyrene particles in this thesis. Thus, we can assume that the acoustic radiation force is dominating and we can neglect streaming forces.

2.7 Coulter Counter

The acoustic mobility of a particle or cell scales with the square of the particle radius. It is therefore important that the mean size and size distribution of the particle is properly measured. This can be done by the Coulter counter method. A schematic is shown in figure 2.9. The particles are suspended in a conducting fluid, which is pumped through a narrow passage between two chambers. In this passage, two electrodes, one on each side of it, measure the electric resistance of the fluid passing through the passage. As a particle passes through the passage, the electric resistance changes. For a spherical particle, the relation between the volume of the particle and the change in resistance is linear. [**18**]
As hundreds of individual particles are measured within seconds it is possible to rapidly observe the distribution curve of the particle size, providing both the average and deviation of the diameter.

In this thesis, the size distribution of four different polystyrene particles of varying advertised size and colour are measured with the Coulter counter.
The measured particle sizes proved to be similar to the information provided by microParticles GmbH (Germany), as shown in table 2.1 and figure 2.9. It is worthwhile pointing out however that the measured standard deviations are significantly larger than the provided standard deviations, although they still deviate less than 15 % from the mean diameter. Due to the low particle count of red 9.89 μm PS beads

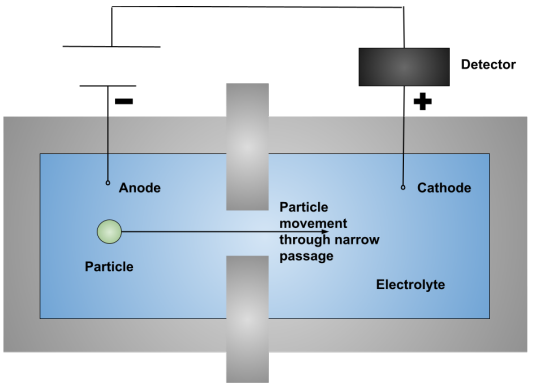

Figure 2.8 As a particle (green) moves through the narrow passage between two chambers, it changes the electrical resistance in the circuit. This change can be used to count the number of cells and measure their size.

Table 2.1 The numerical data obtained from the Coulter counter. The expected values provided by the manufacturer are within the standard deviation of the measurements.

	Count	Mean (μm)	Median (μm)	SD (μm)	d10 (μm)	d90 (μm)
Green 5.18μm PS beads (SD=0.14)	39 853	5.21	5.12	0.63	4.81	5.68
Green 7.81μm PS beads (SD=0.11)	14 002	7.76	7.78	0.69	7.49	8.24
Red 4.99μm PS beads (SD=0.16)	47 356	5.00	4.88	0.69	4.55	5.50
Red 9.89μm PS beads (SD=0.10)	5 713	9.52	9.89	1.56	9.40	10.28

and their large difference from the debris found in each population at around 2 μm, the measured mean particle size decreased whilst the standard deviation increased.

2.8 Contrast Factor Measurement

As described in section 2.4, the acoustic mobility and contrast factor of a particle are measured by tracking their movement towards the node of a standing acoustic wave.

The particles are suspended in a medium with known acoustic properties, which fills the microfluidic device described in section 2.1. The flow is stopped by the

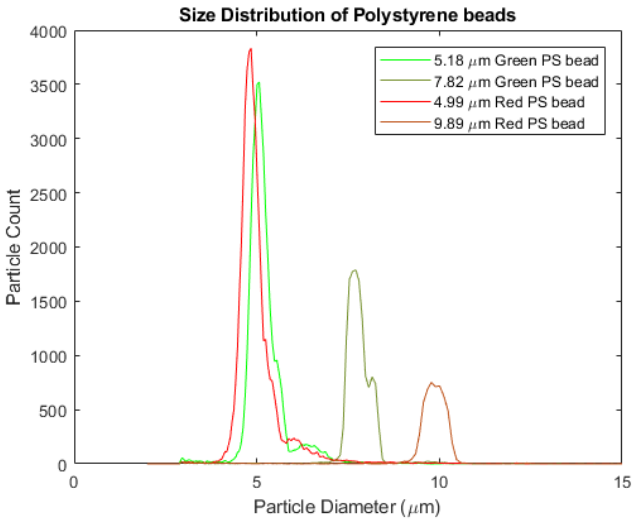

Figure 2.9 Size distribution of the four types of polystyrene particles used in the thesis. Compared to the diameters provided by the manufacturer (MicroParticles GmbH, Germany), the diameters proved to be similar, albeit with a higher standard deviation.

multiport valve.
The particles are suspended randomly in 3D inside the channel. To levitate the particles to a single focal plane, the 5 MHz transducer is activated. This transducer causes a horizontal standing wave with a node at half the height of the channel, as illustrated in figure 2.8.
This step has multiple advantages: Firstly, the microscope only has a certain field of depth, so particles close to the bottom or top of the channel would be out of focus, which negatively affects the particle tracking. Secondly, the particles are all in the same plane and as far away from the bottom and top of the channel as possible, so the wall induced forces are minimised and affect every particle equally. Furthermore, by first levitating all particles to the same plane, the theoretical model needed to describe the movement of the particles is reduced from a movement in a 3D environment into a 1-dimensional movement.
As the particles have levitated to the central plane of the chip, the 5 MHz transducer is deactivated and the 2 MHz transducer is activated in its place. This frequency creates a vertical standing wave, which causes the particles to migrate towards the acoustic node in the centre of the channel, as illustrated in figure 2.8.

As neither the transducers, the chip nor the medium are perfect the exact frequencies that give standing waves can vary with up to 10%, so it is necessary to calibrate

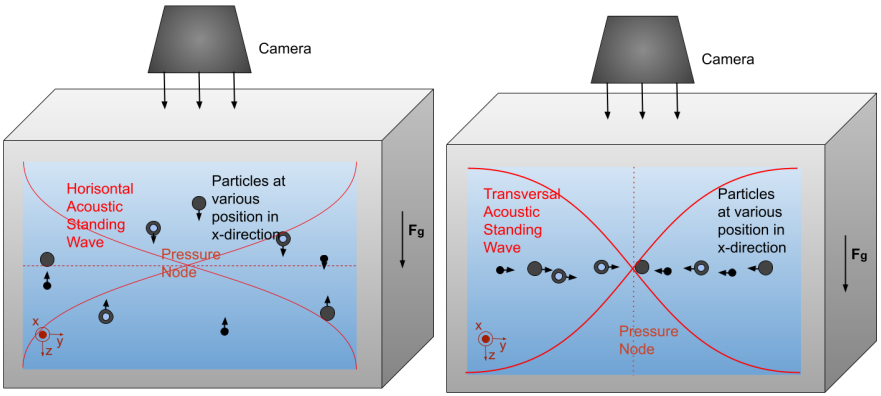

(a) Levitation of the particles to a horizontal plane by the horizontal acoustic standing half wave introduced by the 5 MHz transducer.

(b) Migration of the particles to a transverse plane by the vertical acoustic standing half wave introduced by the 2 MHz transducer.

Figure 2.10 As the particles (black) are subject to the acoustic standing fields they move accordingly. First, they are levitated to the central horizontal plane. (fig. 2.8). Then, the horizontal focusing frequency is replaced by the vertical focusing frequency (fig. 2.8), causing the particles to migrate into a single file row along the channel.

the frequencies until the particles align in a straight, central line. Due to hotspots of acoustic energy density in the channel, this might not be possible, in which case it is advisable to move the field of view to another section along the channel.

As the acoustic energy density in the channel is unknown the movement of reference particles with known acoustic properties needs to be performed prior to each experiment. In this thesis, 5.19 μm green fluorescent PS beads (microParticles GmbH, Germany) are used for this purpose. As the energy density varies along the channel and the contrast factor depends on both the frequency and acoustic energy density it is vital that the unknown particles or cells are measured at the same position along the channel and the same frequencies and voltages as the reference particles.

To obtain a sufficient amount of particle trajectories, the channel needs to be flushed and new particles introduced to the field of view repeatedly. In this thesis, this was done 20 times each experiment.

2.9 Computational Data Analysis

During and after the experiments, multiple programs and scripts were utilised to fit the measurements to the theoretical model and calculate the acoustic energy density as well as the contrast factor.

Micromanager

The MicroManager2.0 program was used to control the exposure and contrast of the camera. The Multi-D-Acq mode of the program took image series of the particle migration with which the particle movement and velocity is calculated.

GDPTlab Script

The GDPTlab script is a Particle Tracking Velocimetry (PTV) GUI written in MatLab by Rune Barnkob. [**26**])
Image series of an acoustic particle migration are loaded into the script which then, frame by frame, tracks the individual particles. The particles are recognised by the software by contrast analysis, using the difference in brightness between the particles due to their fluorescent properties and the dark background. The tracking through each screen results in the particle trajectories shown in figure 2.11.
The script produces a matrix consisting of the velocity and position of the individual particles tracked throughout the image series.

Matlab Scripts

The matrices produced by the PTV software are fitted to the theoretical model and the unknown factors are calculated using a number of custom MatLab scripts according to the flowchart in figure 2.12. The scripts are attached to the end of this chapter for reference.

The first script, called 'Particle Selection', takes the matrices generated from the PTV software and creates individual 'Trajectory'-arrays for each particle. In this script, the position and velocity data is translated into μm and μm/s.

The 'Particle Selection' script is supported by a 'Fetch'- function to load the matrices.

The created trajectories can be used in two different ways.
If the acoustic properties of the particle are known and the trajectories are used as reference to determine the energy density of the channel, they are loaded into the 'Energy Density' - script.
If the acoustic properties of the particle are not known and the goal is to determine

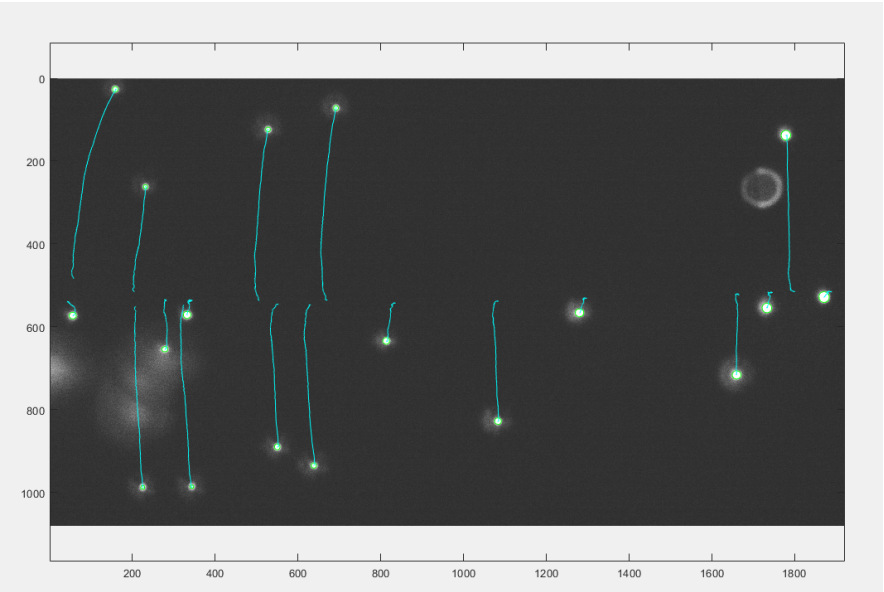

Figure 2.11 The Particle Tracking Velocimetry (PTV) script tracks the fluorescent particles frame by frame and calculates their movement and velocity. The particles (white) moved towards the centre, with the PTV script tracking their movement (turquoise) and creating MatLab data matrices containing their velocity and position. The larger bright spots in the image are due to particles that are stuck on the bottom of the channel.

them, they are loaded into the 'Contrast Factor' - script.

The two scripts both begin by compartmentalising the trajectories into 12 slices, depending on their average position in the field of view. This compartmentalisation and the loading of the trajectories is done in line 1 - 37. Part of the loading is also the exclusion of individual data points that do not have a velocity above a certain threshold (line 17).

The necessary parameters for the fluid, particles and channel are listed and used to calculated f_1, f_2 and Φ_{theory}, with the only difference between the scripts being the inclusion of the calculated acoustic energy density E_{ac} in the 'Contrast Factor' - script.

In the next section of the code, a sinusoidal function is fitted to the velocity profile within each of the slices. With this fitting, it is possible to calculate either the acoustic energy density of the channel within that slice or calculate the contrast factor of

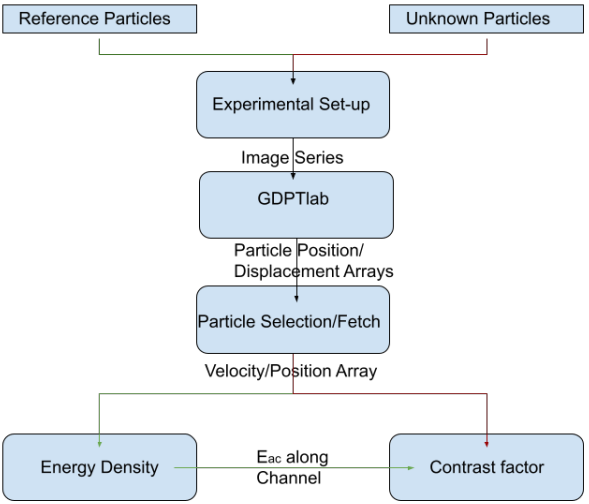

Figure 2.12 The image series of both the reference particles and the unknown particles are processed using the GDPTlab GUI, followed by the 'Particle Selection'-script. The reference particles are used to calculate the acoustic energy density, which in turn is used to calculate the acoustic factor of the unknown particles.

particles moving within the slide, as shown in section 2.6, depending on the script.

The remainder of the script calculates the standard deviation of data points from the sinusoidal fitting: $ASD = \sqrt{\frac{\sum_{i=1}^{N}((D_i - D_{\text{mean}})^2)}{N-1}}$ with D being the closest square distance of the data from the fitted curve. Additionally, the sinusoidal fitting is plotted. Both steps serve as controls for the fitting accuracy.

```
%% Script Name: Particle Selection

framerate=50; %% The framerate of the camera
listing = dir('Data');
q = 0;
for i1=3:length(listing)
listing(i1).name
[Data] = Fetch(i1,listing(i1).name); %%Loading the data matrices
trajec_no=max(Data.ID);
w = dir('*.mat');

for n=1:trajec_no
    Y=Data.Y(Data.ID==n)*(1e-6); %% conversion to micrometres
    Vy=Data.DY(Data.ID==n)*framerate*(1e-6);
    %% conversion to micrometres/second
    X=Data.X(Data.ID==n)*(1e-6);
        q=q+1;
        path=abs(Y(end)-Y(1))*(1e6);
        pathR=round(path,2);
        str=['Trajectories\',sprintf('%01d',q),'.mat'];
        save(str,'Xs','Ys','Vys','path','n'); %%creation of ...
        %% ...Trajectory array
end
disp('end')
end
```

```
%% Script Name: Fetch
function [Data] = Fetch(i1,name )
load(['\Data\' name  ]);

switch i1
    case 1
Data = data1;
    case 2
Data = data2;
...
    case 20
Data = data20;
end
end
```

```
%% Script Name: 'Energy Density' (including comments about
%% differences to the 'Contrast factor'- script)
TracombineSlice1.Y=[];
TracombineSlice1.Vy=[];
...
TracombineSlice12.Y=[];
TracombineSlice12.Vy=[];

XsToCombine=[];

cutPercentageStart=0;
cutPercentageEnd=1;
xCut_1=0.5*10^(-4); %%creation of 50 micrometre wide slices
...
xCut_11=1*10^(-4);

cutOffVel=10^(-6)*10; %%threshold of the velocity filter

N = 100; %%number of Trajectories
for i=1:N
    str=['Trajectories\',sprintf('%01d',i)];
    load(str);
    cutStart=ceil(length(Ys)*cutPercentageStart);
    cutEnd=floor(length(Ys)*cutPercentageEnd);
    for i1=1:length(Ys)  %% sorting of Trajectories into slices...
    %%...and exclusion of low velocity data points
        if (abs(Vys(i1))>cutOffVel)
            if (mean(Xs)<xCut_1)
                TracombineSlice1.Y=[TracombineSlice1.Y Ys(i1)];
                TracombineSlice1.Vy=[TracombineSlice1.Vy Vys(i1)];
                ...
            elseif (mean(Xs)>xCut_11)
                TracombineSlice12.Y=[TracombineSlice12.Y Ys(i1)];
                TracombineSlice12.Vy=[TracombineSlice12.Vy Vys(i1)];
            end
        end
    end
end

%%% Fluid Parameters
rhof=0.997e3; %%fluid density
Cf=1.497e3;   %%fluid speed of sound
vis=0.890e-3; %% viscosity
Kappaf=1/rhof/Cf^2;

%%%% Particle Parameters
rhop=1.05e3; %%particle density
radius=2.602e-6; %%particle radius
Kappap=2.49e-10; %%particle compressibility
%% rhop and kappap not included in the 'Contrast factor'-script
%%%% Channel Parameters
```

```
W=375e-6; %% Channel width
ky=pi/W;  %%wavenumber

%%%% Calculations
Gamma=rhop/rhof;
f=Cf/2/W;
thbou=sqrt(2*vis/rhof/2/pi/f);
Beta=Kappap/Kappaf;
f1=1-Beta;
f2=(2+3*thbou/radius)*(Gamma-1)/(2*Gamma+1+9*thbou/2/radius);
coeffTheory=f1/3+f2/2;

xSlice1=TracombineSlice1.Y;
ySlice1=TracombineSlice1.Vy;

fun=@(a,x) a(1)*sin(2*pi*x/a(2)+a(3)); %% sinusoidal fitting of...
%% ...datapoints using closest square method
sinfitSlice1=lsqcurvefit(fun,[max(ySlice1),W,0],xSlice1,ySlice1);
EacSlice1=3*vis*sinfitSlice1(1)/2/(pi/sinfitSlice1(2))...
/(radius^2)/coeffTheory;
%% In the 'Contrast Factor'-script, replace last line with:
%% coeffSlice1 1=3*vis*sinfitSlice1(1)/2/(pi/sinfitSlice1(2))/...
%% (radius^2)/EacSlice1;
...
xSlice12=TracombineSlice12.Y;
ySlice12=TracombineSlice12.Vy;

fun=@(a,x) a(1)*sin(2*pi*x/a(2)+a(3));
sinfitSlice12=lsqcurvefit(fun,[max(ySlice12),W,0],...
xSlice12,ySlice12);
EacSlice12=3*vis*sinfitSlice12(1)/2/(pi/sinfitSlice12(2))...
/ (radius^2)/coeffTheory;
%% In the 'Contrast Factor'-script, replace last line with:
%% coeffSlice12 1=3*vis*sinfitSlice12(1)/2/(pi/sinfitSlice12(2))/...
%% (radius^2)/EacSlice12;

squaredDistCollectSlice1 = 0; %% normalised squared distance calculation
for i= 1:length(xSlice1)
squaredDistSlice1(i) = ...
((xSlice1(i))-ySlice1(i))*((xSlice1(i))-ySlice1(i))';
squaredDistCollectSlice1 = ...
squaredDistCollectSlice1 + squaredDistSlice1(i);
end
squaredDistNormalizedSlice1 =...
squaredDistCollectSlice1/length(xSlice1);
...
squaredDistCollectSlice12 = 0;
for i= 1:length(xSlice12)
squaredDistSlice12(i) = ...
((xSlice12(i))-ySlice12(i))*((xSlice12(i))-ySlice12(i))';
squaredDistCollectSlice12 = ...
squaredDistCollectSlice12 + squaredDistSlice12(i);
end
squaredDistNormalizedSlice12 =...
```

```
squaredDistCollectSlice12/length(xSlice12);

times = linspace(0,W);
%%For 'Contrast Factor'-script, replace the Eac in the title with...
%%...the Contrast factor.

figure
plot(xSlice1,ySlice1,'ko',times,fun(sinfitSlice1,times),...
'b-','LineWidth',2)
axis([0 W -2*10^(-4) 2*10^(-4)])
title(['Slice 1: Eac =' num2str(EacSlice1) ',...
N = ' num2str(length(xSlice1)) ',...
ASD = ' num2str(squaredDistNormalizedSlice1)])
xlabel('Particle Distance from lower Channel Wall (m)');
ylabel('Particle Velocity (m/s)');
...
figure
plot(xSlice12,ySlice12,'ko',times,fun(sinfitSlice12,times),...
'b-','LineWidth',2)
axis([0 W -2*10^(-4) 2*10^(-4)])
title(['Slice 12: Eac =' num2str(EacSlice12) ',...
N = ' num2str(length(xSlice12)) ',...
ASD = ' num2str(squaredDistNormalizedSlice12)])
xlabel('Particle Distance from lower Channel Wall (m)');
ylabel('Particle Velocity (m/s)');
```

3

Experiments with the Computational Model

The computational model and script in the experiments is novel and had previously shown some limitations. We evaluate different codes and scripts to improve the data processing and analysing.

3.1 Initial Data prior to Thesis

The model and set-up described in this thesis had been developed prior to the beginning of this thesis. However, the model initially showed issues in reproducability and had large deviations within data sets. In table 3.1, 4.9 μm green PS beads are the reference to calculate the contrast factor of 12 μm red beads for different buffer compositions. The measured value for Φ_{PS} differed with -33.73; -37.98; -15.98 and -37.94% from the calculated value for Φ_{PS}.

3.2 Compartmentalisation of Field of View

In the original model used in the early stages of this thesis, the acoustic energy density and contrast factor were calculated by looking at all the trajectories across the entire field of view of the camera, which equals to around 620 μm. Due to this, the model assumes that the acoustic energy field is homogeneous across the entire field of view, but in reality there might be some local variations in strength of the acoustic field along the channel.
During the thesis, this model was instead replaced with a more refined one. The trajectories were sorted into 12 regions depending on the mean position of the trajectory along the field of view. These 50 μm thin slices were then analysed individually instead of analysing the entire field of view.

Table 3.1 The contrast factor of red PS beads was measured using green PS beads as reference. This was done for different buffer solutions of PBS and Ficoll Paque. A theoretical Φ was calculated first, then the acoustic energy density was measured for each particle. The acoustic energy density measured by the green PS beads was then used as input to calculate Φ of the red beads. Finally, the measured Φ is compared to the calculated Φ.

FluoroMax PS	Medium	Φ_{calc}	$E_{ac;fit}$	$E_{ac;input}$	Φ_{calc}	$D_{\%;\Phi}$
Green 4.9	PBS	0.159	6.735			
Red 12	PBS	0.159	4.465	6.735	0.105	-33.73%
Green 4.9	20% FP PBS	0.151	7.297			
Red 12	20% FP PBS	0.151	4.525	7.297	0.094	-37.98%
Green 4.9	40% FP PBS	0.143	8.224			
Red 12	40% FP PBS	0.143	6.912	8.226	0.120	-15.97%
Green 4.9	60% FP PBS	0.135	15.822			
Red 12	60% FP PBS	0.135	9.817	15.822	0.084	-37.94%

To compare the two different models, a data set of trajectories was generated by measuring 5.19 μm green polystyrene particles (microParticles GmbH, Germany) in the experimental set-up described in section 2.6.
This data set was analysed using both the original and the new model, which resulted in the sinusoidal fittings seen in figure 3.1.
As shown in figure 3.2, the large amount of data points make it difficult to determine if the sinusoidal fitting is accurate. Interestingly enough, the standard deviation is similar to the curve fittings of the individual slices, which might be due to the high count of data points.
In figure 3.2 we can see that the sinusoidal fitting of the trajectories varies along the channel, causing differences in the acoustic energy density. This is a strong argument for using the compartmentalised model instead of looking at the complete set of data at once, since the variations of the acoustic energy density along the channel might greatly influence the measurement and calculation of the acoustic contrast factor. Using an average across the entire 620 μm of the field of view is likely to introduce errors in the results. In comparison, analysing the particles in local slices lowers the risk of significant variations in the acoustic energy density. Additionally, it helps in detecting and excluding regions of the field of view that lie within an acoustic energy density hot-spot, as they would show up as large alterations in acoustic energy density between neighbouring slices.

3.3 Velocity Requirement

In the original model, the data points created due to the delay between triggering the time acquisition and the initiation of the migrational acoustic field were excluded

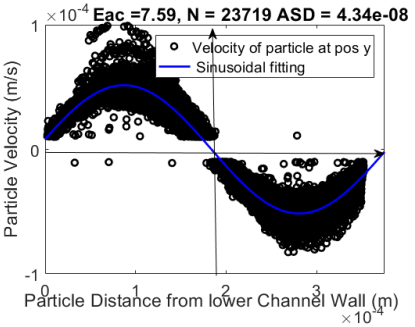

(a) Curve-fitting of entire field of view.

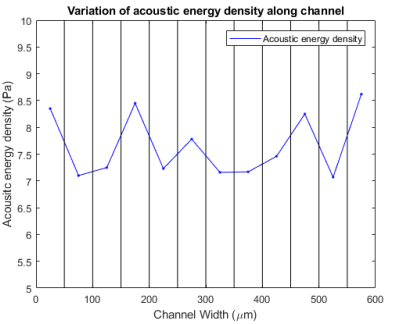

(b) Variation along the channel field of view.

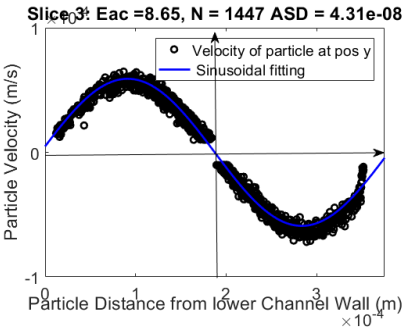

(c) Curve-fitting of Slice 3.

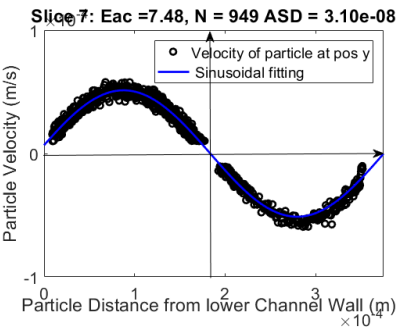

(d) Curve-fitting of Slice 7.

Figure 3.1 In figure 3.2, all particles along the channel were analysed at once. In figure 3.2, the channel had been divided into 12 separate slices and the fitting was done for each slices separately, showcasing how the acoustic energy density differs along the channel. A closer look at two of the slices in figure 3.2 and 3.2 also reveal that the sinusoidal fitting becomes much more narrow and concise as well.

by cutting out the first 20 data points.
In a similar fashion, the last 20 data points were also excluded, as the particle assumable would have completed it's migration to the centre of the channel.
This method is flawed, as the initiation of the time acquisition and the acoustic field are both done manually and the time difference between those events tends to vary between each migration.
Additionally, particles start their migration from vastly different distances away from the centre of the channel, which means that they will have completed their migration at different times, so a static approach to eliminating the data points where migration has been completed is not ideal.

As both of these issues relate to particles that are stationary and do not migrate, the model was updated by introducing a new parameter: a minimum velocity requirement filter. As the trajectories were sorted into the different slices, as introduced in the previous experiment, any data point that had a velocity below a certain threshold was simply excluded. This method excludes data points of stationary particles, which can occur due to the particles attaching to the channel wall or completing their migration.

To test the velocity filter and calibrate it to the appropriate threshold, the same set of trajectories created by the migration of 5.18 μm green polystyrene beads was analysed for 4 different velocity thresholds: 1 μm/s, 5 μm/s, 10μm/s and 50μm/s. An attempt was made at implementing a 100μm/s filter, but it resulted in the elimination of all data points.
As could be expected, the higher the velocity filter is set, the fewer data points remain. Taking a closer look at the produced sinusoidal functions, we can see in figure 3.3 and 3.3 that the sinusoidal fitting does not align well with the data points due to an abundance of errand data points with a velocity close to 0 μm/s. This issue is resolved for velocity filters higher than 10 μm/s, as the errand data points are eliminated (figure 3.3).
For a filter above 50 μm/s most data points that were along the sinusoidal function are eliminated, especially close to the centre of the channel where particle velocities are the lowest. The average standard deviation, ASD, is unaffected by the exclusion of the errand data points, but increases significantly as a majority of the data points are filtered in figure 3.3.

In conclusion, the implementation of a velocity filter is effective in eliminating errand data points and improves the fitting of the sinusoidal function. A velocity filter around 10 μm/s appears appropriate, although this depends on the migrational velocity of the particles and is thus dependent on the particle and medium as well as the strength of the acoustic field. It might thus be of interest to calibrate the filter accordingly for each experiment to obtain the ideal function fitting and subsequently, the most accurate calculation of the acoustic mobility. The model has the drawback that it looses some data points close to the centre and the edges of the channel, as the particles move the slowest in those regions.

3.4 Distance Requirement

In the original model, particles that did not properly migrate due to moving to slowly or getting stuck were eliminated by implementing a travel distance requirement for the particles. This however lead to the exclusion of the majority of trajectories, as particles that started their migration in the central portion of the channel would be completely disregarded. With the implementation of the velocity filter, as described

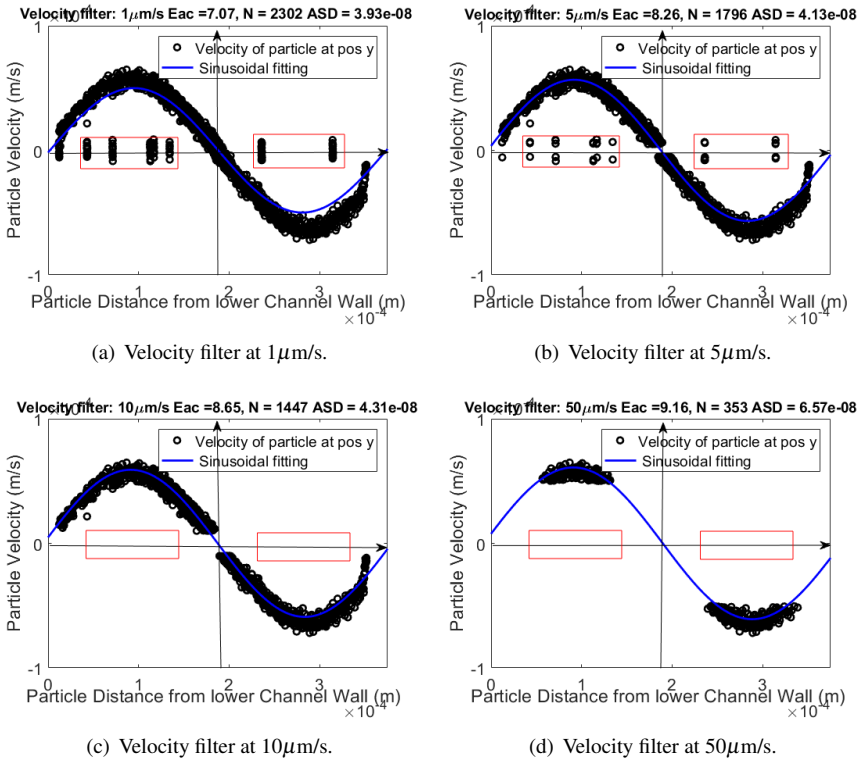

(a) Velocity filter at 1μm/s.

(b) Velocity filter at 5μm/s.

(c) Velocity filter at 10μm/s.

(d) Velocity filter at 50μm/s.

Figure 3.2 Using the same sample and only changing the minimum velocity criteria, the data is fitted to a sine function. As can be seen by comparing 3.3 - 3.3, the data points align differently well to the generated sine function. This is mainly due to the effect of errand data point (red boxes). This fitting becomes, generally speaking, better for higher velocity filters, although their is a point were sections of the function lack any correlating data point, as can be seen in 3.3.

in the previous experiment, the issue of stuck and slowly moving particles is already being addressed in the new model.

To control if the distance requirement has been made obsolete in the new model, the same raw data, produced by measuring the migration of 5.19 μmm green Polystyrene Beads, was used to create four sets of particle trajectories, with a trajectory distance requirement of 0 μm, 20 μm, 50 μm and 100 μm respectively. As could be expected, the number of particle trajectories included decreases as the distance threshold increases, as can be seen in table 3.2.

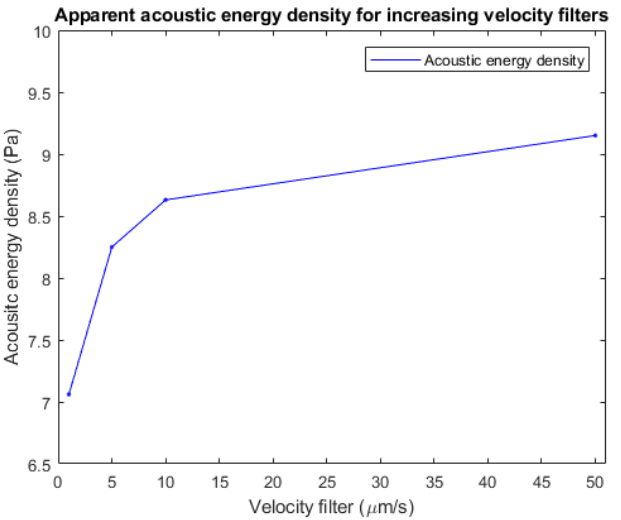

Figure 3.3 Apparent acoustic energy density for increasing velocity filters.

Table 3.2 Number of Trajectories included in analysis for different Distance Filters

Distance Filter	Trajectory Number	Datapoint Number in sinusoidal fitting	Measured E_{ac} (Pa)
0μm	209	1502	8.64
20μm	168	1447	8.63
50μm	133	1363	8.64
100μm	83	1049	8.65

The four sets were analysed with the same, calibrated velocity filter of 10 μms, as discussed in the previous experiment.

As shown in the sinusoidal function fittings in figure 3.4, there does not appear to be a significant impact due to the distance requirements. The function as well as the measured acoustic energy density appear to be almost identical for the various filter settings.

In table 3.2 the number of trajectories in each data set decreased significantly, but the amount of data points in the sinusoidal fitting only lowers slightly as the distance threshold increases. This indicates that the distance requirement filter and the velocity filter target the same trajectories and data points. As with the velocity filter,

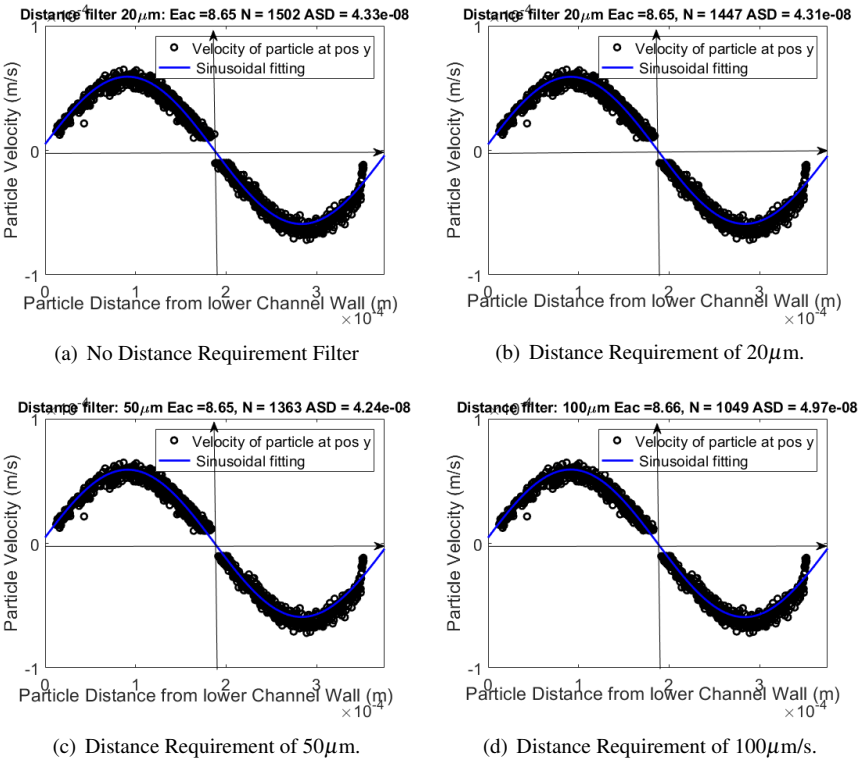

(a) No Distance Requirement Filter

(b) Distance Requirement of 20μm.

(c) Distance Requirement of 50μm.

(d) Distance Requirement of 100μm/s.

Figure 3.4 Using the same sample and only changing the minimum distance travelled criteria, the data is fitted to a sine function. As can be seen by comparing 3.4 - 3.4, the data points of each image are fairly similar and result in very similar values for the energy density of the channel.

.

the average standard deviation remains unaffected by the different distance filters.

We conclude that the distance requirement filter is no longer an effective tool in the model, as it's function is already being fulfilled by the velocity filter, which has a far higher precision since it targets individual data points instead of eliminating entire particle trajectories.

4

Experiments

The direct measuring of particles' and cells' acoustic properties is a fairly novel technology and thus the experimental set-up was in need of a lot of experimentation and calibration in order to achieve calculations of the particles acoustic mobility within an acceptable error margin.

4.1 Position along Channel

To find a section of the channel that has an even acoustic energy density distribution and lacks any hot-spots which might be detrimental to future experiments the channel was initially visually examined. After filling it with a Milli-Q water solution containing fluorescent polystyrene particles, the flow was stopped and the vertical acoustic standing wave was activated, causing the particles to migrate. Along the channel, three separate regions showed the polystyrene particles aligning in a straight line in the centre of the channel. They were marked using a permanent marker, as shown in figure 4.1.

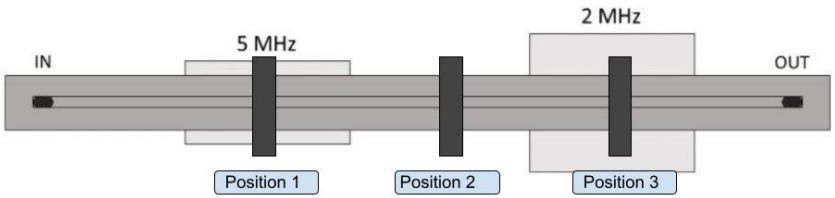

Figure 4.1 The acoustic energy density was measured three times at three different positions along the channel in order to find a stable region for future experiments.

Three independent trials using 7.81 μm green polystyrene beads were then performed for each of the position in order to calculate the acoustic energy densities

and determine which of the positions had the most stable energy density distribution.

Table 4.1 Three independent trials measuring the acoustic energy density E_{ac} at the three positions along the channel as described in figure 4.1.

	E_{ac} (Pa) Position 1	E_{ac} (Pa) Position 2	E_{ac} (Pa) Position 3
Trial 1	1.84	6.49	2.04
Trial 2	3.71	22.94	80.81
Trial 3	1.46	2.07	6.20

The acoustic energy densities for position 2 and 3 described in table 4.1 differ with up to 1000% and 4000% respectively between trials. This leads to the conclusion that there is a hot-spot in acoustic energy density at these position. The values for position 1 are more stable, with a variation of less then 300%.
The measurements, as well as their processing, was performed rather crudely, being the very first measurements performed on the set-up. Due to this there were many mistakes during the measurements increasing the results, such as too high particle concentrations and movement of the chip device. Similarly, the data analysis was performed with the unaltered, preexisting script, further decreasing the accuracy of the measurements.

Position 1 in the experiment appears to be the most suitable for measurements, and experiments within this thesis were performed in that region of the device.

4.2 Self Reference of Polystyrene Particles

After deciding on a position for the measurements, the precision of the method and the reliability of polystyrene beads were examined by using 5.18 μm green fluorescent polystyrene beads (microParticles GmbH, Germany) as reference particles to calculate their contrast factor in a "self-reference"-experiment. A series of four independent experiments using the same acoustic field settings, solution concentration and position along the chip were performed. The resulting image series were then analysed as described in section 2.8, using the first experiment as the reference for itself as well as the other experiments. This self-reference experiment serves as a control that the script works as intended as well as measuring the standard deviation and reliability of the particle, which is vital for its use as the default reference particle in the experiments described in this thesis.

By repeating the experiment three times and measuring the contrast factor in each 50 μm thin slice along the field of view, we gather a total of N = 36 measure-

Table 4.2 The field of view was sequenced into 12 adjacent slices, each 50 μm wide. Using Sample 1 to calculate the energy density at the various slices of the field of view, the energy density was subsequently used to calculate the contrast factor of three additional samples. All samples were measured at the same position along the chip, with a levitation frequency of 4.89 MHz and a migration frequency of 1.96 MHz. The peak to peak voltages in the piezotransducers were kept at 1.27 V_{pp} for the levitation and 1.3 V_{pp} for the migration. The particle concentration was $0.3 \cdot 10^6$ beads/ml suspended in Milli-Q water.

	E_{ac} (Pa)	Φ Sample 1 (ref)	Φ Sample 2	Φ Sample 3	Φ Sample 4
Slice 1	7.96	0.165	0.248	0.163	0.168
Slice 2	9.73	0.165	0.159	0.202	0.149
Slice 3	10.63	0.165	0.173	0.160	0.160
Slice 4	11.61	0.165	0.181	0.148	0.165
Slice 5	13.18	0.165	0.162	0.154	0.163
Slice 6	13.95	0.165	0.169	0.164	0.167
Slice 7	14.64	0.165	0.159	0.172	0.168
Slice 8	13.98	0.165	0.178	0.178	0.185
Slice 9	15.91	0.165	0.157	0.158	0.163
Slice 10	15.65	0.165	0.154	0.164	0.165
Slice 11	16.72	0.165	0.155	0.167	0.162
Slice 12	15.65	0.165	0.160	0.168	0.176
Φmean:	0.167				
SD	0.007				

ments of the contrast factor, as shown in table 4.2. (the first sample was used as a reference and does not contribute). The mean contrast factor was calculated by $\Phi_{\text{mean}} = \frac{1}{N}\sum_{i=1}^{N}(\Phi_i)$ and the standard derivation by $SD = \sqrt{\frac{\sum_{i=1}^{N}((\Phi_i - \Phi_{\text{mean}})^2)}{N-1}}$. From table 4.2 we can conclude that the average mean contrast factor of the measurements was 0.167 with a standard deviation of 0.007, which is very similar to the theoretical value of 0.165.

These results indicate two things:
Firstly, it would appear that the computational model can accurately analyse the given particle trajectories and calculate their contrast factor.
Secondly, the 5.18μm sized green polystyrene beads would serve as a sufficient reference particle, as the low standard deviation indicates that the beads can reliably be used to determine the acoustic energy density in the channel.

4.3 Particle Concentration Differences

Due to the acoustic and hydrodynamic particle-particle interactions, described in section 2.2, the concentration of particles can greatly influence the measurement of their acoustic properties.

To evaluate how much this affects the acoustic mobility measurements we measure the acoustic energy density for particle concentrations at 10^6, $5 \cdot 10^6$, 10^7 and $5 \cdot 10^7$ Particles/ml of 5.19 μm green PS beads, keeping all other experimental parameters static.

The experiment was repeated two times, each time at a different position along the channel to avoid any biases. The measured apparent acoustic energy density is displayed in table 4.3.

Table 4.3 The measured acoustic energy density depending on the particle concentration shows that the apparent acoustic energy density begins to increase above a threshold concentration between $5 \cdot 10^6$ and 10^7.

Particle Concentration (N/ml)	$E_{ac}(Pa)$ Position 1	$E_{ac}(Pa)$ Position 2	$E_{ac}(Pa)$ Position 3
10^6	3.40	7.30	9.80
$5 \cdot 10^6$	3.21	7.33	9.45
10^7	3.70	8.26	11.23
$5 \cdot 10^7$	5.00	10.14	14.12

The experiment shows that the apparent acoustic energy density increases for higher concentrations of particles. This indicates that the particles begin to interact with each other at higher concentrations, pulling each other along and thus moving faster than they would otherwise. This behaviour can be explained by hydrodynamic particle-particle interactions.

According to Leys et al., an average distance between particles larger than two times their diameter is recommended to avoid these hydrodynamic effects. [**14**]

The average distance can be calculated by assuming that the particles are evenly distributed. Due to the levitation, the particles are all suspended on a plane, with an average distance between their centres, d_{avg}, as shown in figure 4.2.

The total particle number N in the channel is described by the particle concentration C_N and the volume V,

$$N = C_N V = C_N wlh, \tag{4.1}$$

with l the length, w the width and h the height of the channel. N is also described

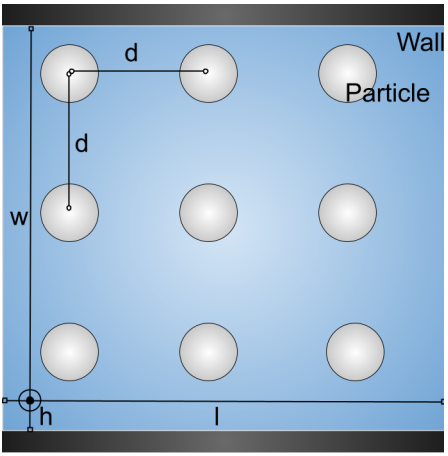

Figure 4.2 Assuming that the particles are evenly distributed in a plane after being levitated, the average distance d between the particles becomes a function of the dimensions of the channel and the particle concentration.

by their average distance and the dimensions of the plane:

$$N = \frac{wl}{d^2}. \tag{4.2}$$

Combining the equations of the particle number gives us

$$C_{\mathrm{N}} wlh = \frac{wl}{d^2} \tag{4.3}$$

such that

$$d = \sqrt{\frac{1}{C_{\mathrm{N}} h}}. \tag{4.4}$$

For a particle concentration of 10^6 N/ml = $10^6 \mathrm{N}/\mu\mathrm{m}$ and a channel height of 150μ, the average distance between the centre of particles is 81.65μm, which means that particles up to 81.65/3 = 27.21 μm can be used at this concentration without taking hydrodynamic interactions into account. Note that the inclusion of the diameter in the average distance is being accounted for by dividing with 3 instead of 2.
For a concentration of $10 \cdot 10^6 \mathrm{N}/\mu\mathrm{m}$, this average distance decreases to 25.82 μm. This is larger than the critical mean distance of 15.6 μm for the polystyrene particles used in this experiment. As we could start to observe changes in the apparent acoustic energy density for these concentrations, it would be advisable to have a larger margin for our mean particle distances than proposed by Leys. This is due the particles not being completely evenly distributed in an experimental set-up, causing particles to sometimes go below the recommended threshold.

4.4 Control of Size Bias

The size of the particles is a vital parameter for the computational model in this thesis. Since the size of the particles and cells that this model eventually wants to evaluate the acoustic properties of can vary from less than 5 μm up to 20-30 μm it is of importance that there is no size bias in the model. In this experiment, two solutions with fluorescent green polystyrene particles from the same manufacturer are used, with 5.18 μm beads functioning as reference particles to calculate the acoustic energy density, which then is used to calculate the contrast factor of 7.8 μm beads. We would expect the particles to have the same contrast factor. In this calculation, the error due to variations in the particle radius is not being accounted for, as a^2 is factored out from the measurements, converting the acoustic mobility $a^2\Phi$ to the size-independent contrast factor Φ, which is necessary for a direct comparison of particles with different sizes.

Table 4.4 The field of view was sequenced into 12 adjacent slices, each 50 μm wide. Using 5.18 μm green PS beads as reference particles to calculate the energy density at the various slices of the field of view, the energy density was subsequently used to calculate the contrast factor of three 7.81 μm green PS bead samples. All samples were measured at the same position along the chip, with a levitation frequency of 4.89 MHz and a migration frequency of 1.96 MHz. The peak to peak voltages in the piezotransducers was kept at 1.27 V_{pp} for the levitation and 1.3 V_{pp} for the migration. The particle concentration was $0.3 \cdot 10^6$ particles/ml for the reference particles and 10^6 particles/ml for the 7.81 μm Green PS beads, each suspended in Milli-Q water.

	Φ Reference	E_{ac} (Pa)	Φ Sample 1	Φ Sample 2	Φ Sample 3
Slice 1	0.165	8.13	0.169	0.153	0.165
Slice 2	0.165	8.29	0.166	0.168	0.157
Slice 3	0.165	8.39	0.154	0.163	0.167
Slice 4	0.165	8.95	0.150	0.147	0.157
Slice 5	0.165	8.53	0.151	0.155	0.158
Slice 6	0.165	8.49	0.137	0.163	0.155
Slice 7	0.165	8.41	0.134	0.152	0.172
Slice 8	0.165	8.59	0.134	0.146	0.166
Slice 9	0.165	8.31	0.147	0.140	0.173
Slice 10	0.165	8.60	0.134	0.133	0.158
Slice 11	0.165	8.12	0.140	0.132	0.160
Slice 12	0.165	8.00	0.159	0.120	0.155
Φ_{mean}	0.153				
SD	0.010				

The calculated contrast factor of polystyrene is 0.165, as shown in section 2.6.

Assuming that the reference particles in this experiment had the theoretical contrast factor, the contrast factor of the 7.82 μm PS particles was calculated to be, on average, 0.153, with some variation across the different samples and slices, as can be seen in table 4.4. This is within a 10 % error margin, which is an acceptable error considering that there are some inherent variations in the particle sizes as well, which was shown during the Coulter counter experiment (table 2.1) in section 2.7.
This indicates that the computational model as well as the measurement methods are fairly accurate and that there doesn't appear to be a size bias.
Of course, this conclusion is based on comparing only two different sizes, and it might be of interest to do a more elaborate study involving several other sizes of the same particle to confer that there is no size bias and create a size/divergence graph.

4.5 Control of Particle Colouring

Based on experiments prior to this thesis there was some empirical data suggesting polystyrene particles that had undergone different staining procedures (some being stained green and some red) do not have the same acoustic properties despite being the same material, which could indicate that the staining process done by the manufacturer might change the properties of the particles, such as the density or the compressibility.
To evaluate this, the contrast factor of 5.0 μm, red fluorescent PS beads and 9.9 μm red PS beads were calculated using 5.18 μm green PS beads as a reference.
As can be seen in tables 4.5 and 4.6, the red beads showed significantly different acoustic properties than the expected 0.165.
For the 4.99 μm, red PS beads the average acoustic factor was calculated to be 0.197, with a standard deviation of 0.008.
For the 9.89 μm Red PS beads the average acoustic factor was calculated to be 0.134, with a standard deviation of 0.003.

These results confirm the observations made prior to this thesis, indicating that the staining of the polystyrene beads or other unknown factors in the manufacturing process causes the acoustic properties of polystyrene to change.
This has further implications, as it would mean that the theoretical contrast factor for polystyrene beads that had been calculated in section 2.6 is likely to not be accurate for the reference particles in this thesis, and it might be of interest to evaluate different approaches within the model to take this into account. One such way would be to instead use glass beads, as they tend to be more homogeneous than polystyrene beads. The various polystyrene particle sizes are fairly well consistent within their population, so if the same reference particle is used, it is still possible to measure the acoustic mobility ratio of cells and particles.

Table 4.5 The field of view was sequenced into 12 adjacent slices, each 50 μm wide. Using 5.18 μm green PS beads as reference particles to calculate the energy density at the various slices of the field of view, the energy density was subsequently used to calculate the contrast factor of three 4.99 μm Red PS bead samples. All samples were measured at the same position along the chip, with a levitation frequency of 4.89 MHz and a migration frequency of 1.96 MHz. The peak to peak voltages in the piezotransducers were kept at 1.27 V_{pp} for the levitation and 1.3 V_{pp} for the migration. The particle concentration was $0.3 \cdot 10^6$ Particles/ml for both the reference particle and the 4.99 μm Red PS beads, each suspended in Milli-Q water.

	Φ Reference	E_{ac} (Pa)	Φ Sample 1	Φ Sample 2	Φ Sample 3
Slice 1	0.165	10.31	0.199	0.219	0.212
Slice 2	0.165	9.94	0.190	0.213	0.190
Slice 3	0.165	10.91	0.173	0.202	0.203
Slice 4	0.165	11.20	0.188	0.185	0.200
Slice 5	0.165	11.66	0.192	0.202	0.214
Slice 6	0.165	9.98	0.192	0.198	0.207
Slice 7	0.165	9.91	0.186	0.206	0.192
Slice 8	0.165	10.34	0.187	0.192	0.187
Slice 9	0.165	9.68	0.188	0.193	0.174
Slice 10	0.165	9.11	0.184	0.192	0.199
Slice 11	0.165	9.04	0.198	0.213	0.202
Slice 12	0.165	8.18	0.188	0.200	0.202
Φ_{mean}	0.197				
SD	0.008				

An interesting observation is that whilst the 4.99μm Red PS beads had a contrast factor 20% higher than expected, the 9.89μm Red PS beads instead had a contrast factor 20% lower than expected.

4.6 Acoustic Mobility Ratio

According to the measurements of the contrast factor of polystyrene particles in this thesis, there are some significant differences between the different sizes and stainings.

To verify whether this is accurate or due to errors in the method an independent experiment is performed in cooperation with another master thesis student, Linda Péroux. The experiment measures the ratio of acoustic mobility between the particles by analysing the relative migration distance of the particles in a chip device. The method and theory was derived by Thierry Baasch.

Table 4.6 The field of view was sequenced into 12 adjacent slices, each 50 μm wide. Using 5.18 μm green PS beads as reference particles to calculate the energy density at the various slices of the field of view, the energy density was subsequently used to calculate the contrast factor of three 9.89 μm Red PS bead samples. All samples were measured at the same position along the chip, with a levitation frequency of 4.89 MHz and a migration frequency of 1.96 MHz. The peak to peak voltages in the piezotransducers were kept at 1.27 V_{pp} for the levitation and 1.3 V_{pp} for the migration. The particle concentration was $0.3 \cdot 10^6$ particles/ml for the reference particles and $0.2 \cdot 10^6$ particles/ml for the 9.89 μm Red PS beads, each suspended in Milli-Q water.

	Φ Reference	E_{ac} (Pa)	Φ Sample 1	Φ Sample 2	Φ Sample 3
Slice 1	0.165	13.15	0.121	0.122	0.134
Slice 2	0.165	12.87	0.135	0.151	0.137
Slice 3	0.165	13.51	0.142	0.138	0.129
Slice 4	0.165	12.45	0.137	0.137	0.123
Slice 5	0.165	13.14	0.137	0.123	0.117
Slice 6	0.165	13.69	0.136	0.145	0.129
Slice 7	0.165	12.50	0.141	0.140	0.128
Slice 8	0.165	12.13	0.137	0.142	0.123
Slice 9	0.165	11.76	0.137	0.136	0.125
Slice 10	0.165	11.03	0.140	0.139	0.137
Slice 11	0.165	11.02	0.134	0.130	0.135
Slice 12	0.165	9.82	0.141	0.146	0.141
Φ_{mean}	0.134				
SD	0.003				

The chip device in this experiment is of the same type that would be used for the separation of particles by acoustophoresis. It consists of a prefocusing channel and a separation channel, each controlled by a piezotransducer. The device has two inlets, one for the prefocusing and one for the main separation channel as well as two outlets, as shown in figure 4.3.
A particle that enters the prefocusing channel will be focused towards the side of the channel due to the two-node acoustic standing wave present. This is done for all particles to have the same lateral position and distance from the centre as they enter the main separation channel There, they are subject to a single node acoustic standing wave and begin to migrate towards the centre of the channel. If the particle's acoustic mobility is sufficiently large, it will be able to move far enough towards the centre to exit the device through the first outlet. If it is still in the outer regions of the channel after leaving the acoustic field it will instead exit through the secondary outlet. The trajectory of a particle in both cases is illustrated with a green and yellow line respectively in figure 4.3.

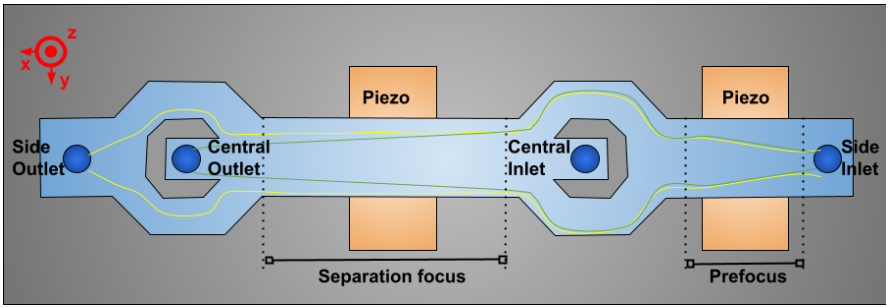

Figure 4.3 The trajectory of the particles with higher (green line) and lower (yellow line) acoustic mobility are first focused to the same lateral position in the prefocus and are then separated by acoustophoresis in the separation focus channel.

The velocity of a particle with size a_1 and contrast factor Φ_1 in the separation channel is a combination of its lateral movement due to acoustophoresis and its movement along the channel due to the flow rate of the medium. It can be described by

$$E_{\text{ac}}\Delta x\Phi_1 a_1^2 = \int_{y_0}^{y_{e1}} [-\frac{3}{2}\frac{\eta}{k}\frac{v_x(y)}{sin(2ky)}]dy. \tag{4.5}$$

Similarly, the movement of a particle with a_2 and Φ_2 can be described with

$$E_{\text{ac}}\Delta x\Phi_2 a_2^2 = \int_{y_0}^{y_{e2}} [-\frac{3}{2}\frac{\eta}{k}\frac{v_x(y)}{sin(2ky)}]dy. \tag{4.6}$$

The ratio of the movement of these particles can thus be described as

$$\frac{\Phi_1 a_1^2}{\Phi_2 a_2^2} = \frac{\int_{y_0}^{y_{e1}} [-\frac{3}{2}\frac{\eta}{k}\frac{v_x(y)}{sin(2ky)}]dy}{\int_{y_0}^{y_{e2}} [-\frac{3}{2}\frac{\eta}{k}\frac{v_x(y)}{sin(2ky)}]dy}. \tag{4.7}$$

Therefore, the ratio of acoustic mobility is calculated by measuring the positions y_0, y_{e1} and y_{e2}. Which is shown in figure 4.4.
The experiment is repeated for ratios between the four different. The mobility ratios of 4.99 μm Red/5.18 μm and 7.82 μm/9.89 μm were not possible to be measured due to their similar sizes.
To compare the contrast factors measured by Particle Tracking Velocimetry with these results the contrast factors were multiplied by the radius of the particle squared, as the mobility ratio is Φa^2.

The theoretical mobility ratio between the particles assuming that Φ would be constant was calculated as a reference point. The ratios are compared in figure 4.5.

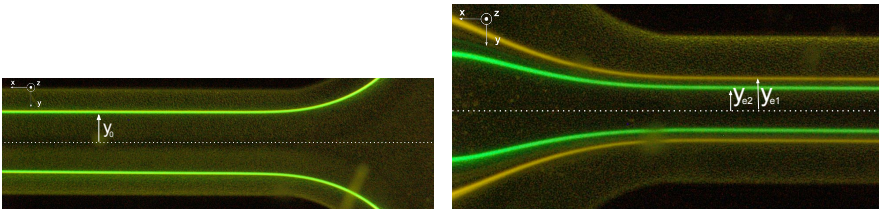

(a) In the beginning of the separation channel, the particle streams are at the same lateral position y_0.

(b) At the end of the separation channel, the particle streams are at different lateral positions y_{e1} and y_{e2}.

Figure 4.4 Two particles (in this experiment 7.81 μm green and 4.99 μm Red PS beads) migrate at different rates in the same acoustic field. The difference in end positions is used to calculate the difference in acoustic mobility. Experiments performed by Linda Péroux.

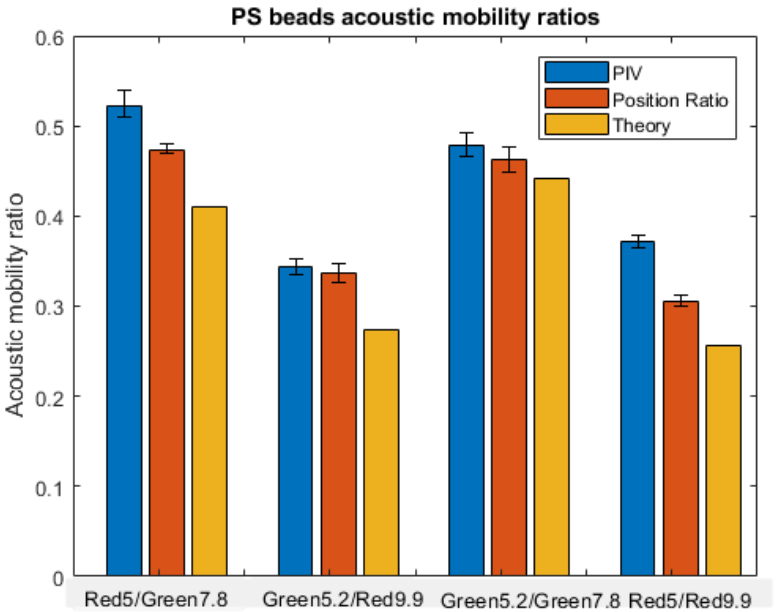

Figure 4.5 The mobility ratios of various polystyrene beads as measured with PTV, the relative migration method and the calculated value assuming a constant contrast factor.

The mobility ratios obtained by the Particle Tracking Velocimetry as well as the relative migration method compared to the theoretical ratios based solely on their size differences show that the measurements are significantly more similar to each other than the theoretical values.

This indicates that the observed variations of the contrast factor are not due errors in the method.

4.7 Polystyrene Contrast Factor Summary

Having measured four different polystyrene particles, and having confirmed the values with an independent experiment, we sum up our results thus far. As we can see from table 4.7 and figure 4.6, there is a significant difference in the measured contrast factors of the different polystyrene particles. This indicates that there are significant differences in the acoustic properties of polystyrene beads.

We can also conclude that without further verification of the particle properties it would not be possible to confidently determine the acoustic properties of unknown particles with polystyrene particles as reference. The major application of the method described in this thesis is however the measurement of two unknown particles relative to each other to determine whether they can be separated. This can still be done by measuring both particles with the same reference particle. With a common reference, it is possible to analyse the ratio in acoustic mobility between the two unknown particles.

Table 4.7 Summary of the acoustic contrast factor and mobility of measured polystyrene beads.

	Diameter (μm)	Size SD (μm)	Trajectory Number N	Contrast factor Φ	SD Contrast factor Φ	Acoustic mobility
Green 5.19	5.21	0.63	865	0.167	0.007	1.134
Green 7.81	7.78	0.69	919	0.153	0.010	2.297
Red 4.99	5.01	0.69	799	0.197	0.008	1.231
Red 9.89	9.52	1.56	307	0.134	0.003	3.043

4.8 Glass Particle Comparison

Based on the results of the particle colouring due to polystyrene being a polymer, it can be assumed that polystyrene has a certain variation in density and compressibility. Thus, it is of interest to evaluate an alternative reference particle with more

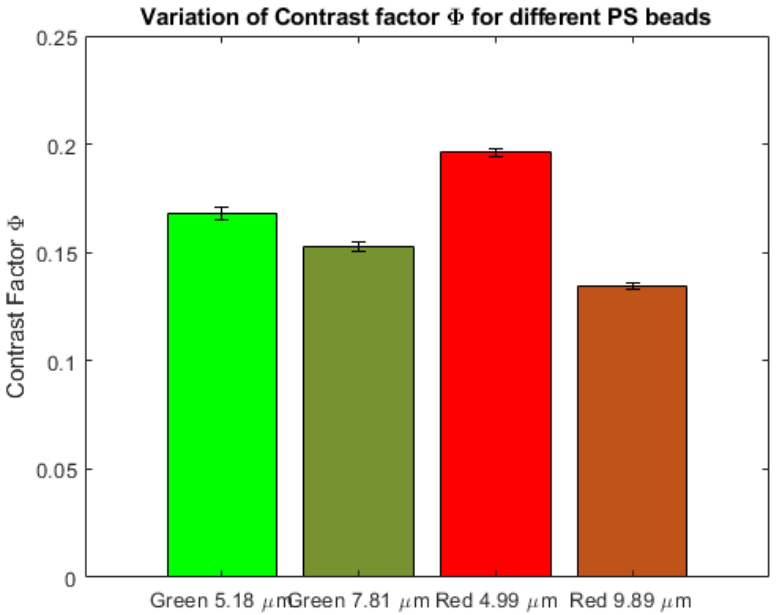

Figure 4.6 The contrast factor of 5.19 μm green PS beads was assumed to be 0.165 as found in literature. With this, the contrast factor of other PS beads was measured, showing significant differences.

homogeneous properties.

silicon glass particles are more internally homogeneous and dense than polystyrene, making them rigid and heavy. Because of this, small errors and variations in the material properties lead to very small errors in the contrast factor, which is not true for polystyrene. Additionally, they have certain surface properties that are beneficial for biological applications and comparisons. To measure their variance, 4 μm red-stained silicon beads (KiskerBiotech GmbH & Co. KG, Germany) were evaluated in the same way as the 5.19 μm green PS beads, as described in section 4.3.
During the experiment, it became apparent that the glass beads were only weakly fluorescent, which caused issues for the tracking software by making it hard to differentiate between the particles and the background noise. This is illustrated in figure 4.7. Due to this, the self-reference experiment resulted in fairly large standard deviations, as can be seen in table 4.8. Compared to the self-reference measurements previously performed with polystyrene particles (Table 4.2), the relative standard deviation is about 10% instead of 4%, a significant deterioration in quality.

Table 4.8 The field of view was sequenced into 12 adjacent slices, each 50 μm wide. Using Sample 1 to calculate the energy density at the various slices of the field of view, the energy density was subsequently used to calculate the contrast factor of two additional samples of the 4 μm fluorescent red silicon glass beads. All samples were measured at the same position along the chip, with a levitation frequency of 4.89 MHz and a migration frequency of 1.96 MHz. The effective voltage in the piezotransducers was kept at 1.27 V_{pp} for the levitation and 1.3 V_{pp} for the migration. The particle concentration was $1.8 \cdot 10^6$ particles/ml suspended in Milli-Q water.

	E_{ac} (Pa)	Φ Sample 1 (ref)	Φ Sample 2	Φ Sample 3
Slice 1	2.80	0.588	0.470	0.714
Slice 2	3.94	0.588	0.489	0.505
Slice 3	4.57	0.588	0.578	0.365
Slice 4	4.90	0.588	0.538	0.481
Slice 5	4.99	0.588	0.536	0.512
Slice 6	5.21	0.588	0.574	0.560
Slice 7	7.31	0.588	0.366	0.516
Slice 8	6.02	0.588	0.647	0.540
Slice 9	6.42	0.588	0.666	0.535
Slice 10	6.31	0.588	0.502	0.648
Slice 11	7.07	0.588	0.542	0.492
Slice 12	6.59	0.588	0.580	0.545
Φ_{mean}	0.555			
SD	0.053			

Because of this, it can be concluded that with the current set-up, silicon glass beads are not suitable reference particles for determining the contrast factor of other particles and cells. Interestingly enough, the glass particles remained only weakly fluorescent even after an optical cable, which was causing issues with the imaging, was replaced.

4.9 Melamine Resin

In this experiment, the acoustic mobility and contrast factor of 5 μm fluorescent green melamine resin, another polymer similar to polystyrene, was measured using 5.18 μm fluorescent green polystyrene particles as reference. Melamine has a density of 1500 kg/m^3, which is significantly higher than polystyrene. [**27**]
Thus we expect the acoustic mobility and the contrast factor to be higher than the reference particles'.
From table 4.9 we can see that the calculated contrast factor of melamine is 0.24, which is significantly larger than the contrast factor of polystyrene. Using the par-

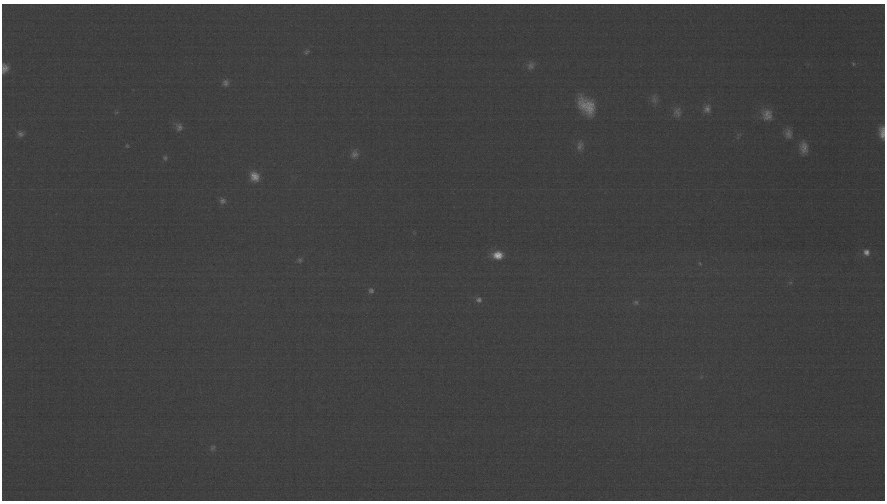

Figure 4.7 A snapshot of silicon glass beads inside the acoustic channel. Due to issues with the camera, the contrast of the particles is too low for accurate tracking.

ticle diameter provided by the manufacturer, 5 μm, we can calculate the acoustic mobility of melamine to be 1.48.

To have an additional point of comparison, the relative acoustic mobility ratio of melamine compared to 9.89 μm Red PS beads was measured using their lateral position in a particle stream as described in section 4.6.

We measured the acoustic mobility ratio to be 0.580, with a 95% confidence interval of 0.569 - 0.591. The acoustic mobility ratio calculated from the PTV contrast factor set-up is 0.449, with a 95% confidence interval of 0.434 - 0.467.

Furthermore, we can use the particle data measured by Cushing et. al. to calculate the contrast factor of melamine. [**27**] In the experiments performed in Cushing's paper the density of melamine resin is determined to be $\rho_{mel} = 1500\text{kg/m}^3$ and the compressibility to be $\kappa_{mel} = 124\text{TPa}^{-1}$. Assuming a fluid density $\rho_0 = 997\text{kg/m}^3$ and a fluid compressibility $\kappa_0 = 448\text{TPa}^{-1}$ we can calculate the contrast factor for melamine, ϕ_{mel}:

$$\phi_{mel} = \frac{1}{3}(1-\bar{\kappa}) + \frac{\bar{\rho}-1}{2\bar{\rho}+1} = 0.367, \tag{4.8}$$

neglecting the viscous terms.

This is a significant difference, although are in an expected spectrum, having a

Table 4.9 The field of view was sequenced into 12 adjacent slices, each 50 μm wide. Using 5.18 μm Green PS beads as reference particles to calculate the energy density at the various slices of the field of view, the energy density was subsequently used to calculate the contrast factor of three melamine samples. All samples were measured at the same position along the chip, with a levitation frequency of 4.89 MHz and a migration frequency of 1.96 MHz. The peak to peak voltages in the piezotransducers were kept at 1.27 V_{pp} for the levitation and 1.3 V_{pp} for the migration. The particle concentration was $0.3 \cdot 10^6$ particles/ml for the reference particles and $0.4 \cdot 10^6$ particles/ml for the melamine particles, each suspended in Milli-Q water.

	Φ Reference	E_{ac} (Pa)	Φ Sample 1	Φ Sample 2	Φ Sample 3
Slice 1	0.165	6.9395	0.2204	0.2395	0.2424
Slice 2	0.165	7.0271	0.2170	0.2410	0.2122
Slice 3	0.165	7.0004	0.2226	0.2476	0.2278
Slice 4	0.165	7.3796	0.1983	0.2316	0.2132
Slice 5	0.165	6.7062	0.2515	0.2801	0.2254
Slice 6	0.165	6.9044	0.2021	0.2421	0.2202
Slice 7	0.165	6.1184	0.2129	0.2552	0.2455
Slice 8	0.165	5.8335	0.2349	0.2451	0.2561
Slice 9	0.165	5.4858	0.2207	0.2390	0.2630
Slice 10	0.165	5.2439	0.1898	0.2543	0.2011
Slice 11	0.165	3.2389	0.3162	0.3181	0.2992
Slice 12	0.165	4.0896	0.1916	0.2457	0.2083
Φ_{mean}	0.236				
SD	0.013				

contrast factor higher than polystyrene but significantly smaller than glass beads. These differences could be due to many reasons, for example, the use of particles from different manufacturers or changes to the polymer due to the staining. The methods of measurement are also widely different and it is in the current stage difficult to determine which method is more accurate and appropriate to determine the acoustic properties of particles.

4.10 Breast Cancer Cells

The most interesting application for the model developed during this thesis is measuring the acoustic mobility of cells. This was performed for three different breast cancer cell lines: BT-20, BT-549 and MCF-7. The experiments as well as the necessary cell cultivation, harvesting and staining were performed in cooperation with

another master thesis student, Simon Olsson.

BT-20 were derived from a 74-year-old human female in 1958. The cells originate from a triple-negative breast cancer caused by an invasive ductal carcinoma in the mammary gland.[**28**]
BT-549 cells are epithelial cells derived in 1978. They originate from a papillary, invasive ductal tumour. [**29**]
MCF-7 are epithelial cells isolated from the breast tissue of a 69-year-old White woman in 1970 with metastatic adenocarcinoma.[**30**]

Cell Staining

As the imaging equipment in both the ImageStream flow cytometry and the acoustic mobility set-up relies on fluorescence, the cells were stained with Calcein AM according to the protocol provided by the manufacturer, Invitrogen. Calcein AM is a fluorescent cell-permeant dye.

ImageStream

As the cells would not have a uniform size throughout their population, we measured the size distribution. Unfortunately, the Coulter counter previously used in this thesis was broken. Instead, the size measurements were performed using ImageStream flow cytometry instead.

In ImageStream flow cytometry, the cells are hydrodynamically focused into a glass cuvette and illuminated by a laser. Fluorescent transmitted and scattered light is collected, from which the software extrapolates cell data.

Repeating this measurement for the three cells resulted in the size distributions seen in figure 4.8.

Acoustic Mobility

Since cells start to disintegrate when suspended in water the measurement of the acoustic mobility was performed with phosphate-buffer saline (PBS) instead. The calcein AM dye staining the cells is green fluorescent to avoid remnant polystyrene beads interfering with the particle tracking. The reference particles were 5.0 μm red PS beads. Tracking and analysing the cells, assuming that the particle size was the mean size measured with ImageStream, we obtain the average contrast factors and acoustic mobilities displayed in table 4.10. See the appendix for the complete contrast factor measurements for each experiment and each cell line.

From this, we can see that the contrast factor and acoustic mobility of BT-549 and MCF-7 cells are very similar to each other whilst the contrast factor and acoustic

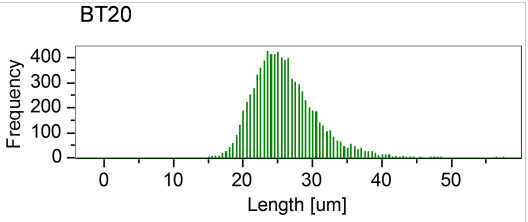

Length [um]

Population	Count	Mean	Median	Std. Dev.
BT20	8409	26.21	25.5	5.858

(a) Size distribution of BT-20 cells.

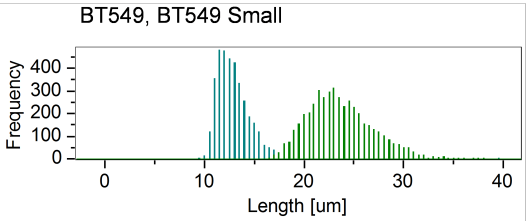

Length [um]

Population	Count	Mean	Median	Std. Dev.
BT549	4592	23.84	23.5	4.399
BT549 Small	3621	13.22	12.5	3.39

(b) Size distribution of BT-549 cells.

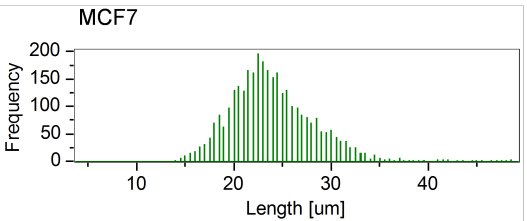

Length [um]

Population	Count	Mean	Median	Std. Dev.
MCF7	3264	24.42	23.5	6.447

(c) Size distribution of MCF-7 cells.

Figure 4.8 The size distribution of the breast cancer cells show that they overlap significantly, with slight differences in the mean and median sizes.

mobility of BT-20 is significantly lower. This indicates that it should be possible to separate BT-20 cells from the other two cell lines with acoustic separation tech-

Table 4.10 The contrast factor and acoustic mobility of cancer cells were measured, showing significant differences between the cells.

	Diameter (μm)	Size SD (μm)	Trajectory Number	Contrast factor	Contrast factor SD	Acoustic mobility
BT-20	26.2	5.86	369	0.004	0.001	0.687
BT-549	23.8	4.40	338	0.009	0.003	1.279
MCF-7	24.4	6.48	268	0.010	0.003	1.476

niques.

5

Conclusions

In this thesis, the main goal was to improve upon a computational model as well as an experimental procedure to accurately determine the acoustic factor of particles and cells. The impact and overall results of the various chapters of this thesis are described below.

The computational model, which describes the data processing and calculations from the obtained particle data is the key to the thesis' intended goals. Whilst the initial model failed in reliably give accurate values for the particles acoustic properties, the new model now can reproduce the same results within an error margin of less than 10 %, which should be reliable enough to achieve fairly good measurements of particles in the system. Two main features led to these improvements.

The first is the compartmentalisation of the data into fairly thin slices, which counteracted the variations of acoustic energy density along the measured region and thus making it possible to measure the particle movement in a more localised way. There are of course some limitations to this. For instance, should the particles not have come to a complete stop when the flow through the channel was stopped, they might be drifting through several slices, but the model would assume that the same conditions of their original position apply. This might be counteracted by having a more extensive code that compartmentalizes each individual data point instead of the entire particles' trajectory. There might be some possible optimisation as well, as the thickness of the slices was chosen rather arbitrarily in this thesis and it could be possible to further improve the sine-function fitting by altering this thickness and the number of slices.

The second was the introduction of a velocity filter, which greatly reduced the number of errant data points and improved the sine function fitting. In this filter, just as with the compartmentalisation, there are some minor detriments. For example, the loss of data points towards the very edges and towards the centre of the sine-function.The data fitting is greatly improved, which by far outweighs the drawbacks. As the velocity depends on various factors, for example the particle size

and the acoustic energy density, it is not possible to give a definite, static value for this filter, but it might be necessary to calibrate it for each experiment.

The experiments in this thesis had the main objective to evaluate and improve the set-up and to find a reliable method to measure the acoustic properties of particles. For that, a lot of attention was put on the fluorescent polystyrene beads, as they were intended to serve as the reference particle in any future development and experiment. They were chosen because they were easily attainable, had already known acoustic properties and can be measured under the same conditions as cells. The initial tests with the coulter measurement showed that their sizes corresponded well enough with the data published by the manufacturer. Evaluating them as reference particles and measuring them in the set-up showed a few things. Firstly, it would appear that the staining of the particles might have had some effect on the acoustic properties of the particles, as differently stained particles (green and red) resulted in different measured contrast factors. The particles in themselves proved to be easy to handle and image, especially compared to attempts using fluorescent silicon glass beads, which were barely visible in the fluorescent microscope and thus hard to track in the PTV program, resulting in worse fitting compared to the polystyrene beads.

The findings that the differently coloured polystyrene beads have different properties also indicates that it is likely that neither the green nor the red-stained particles have the same contrast factor as assumed from calculations, which raises issues when using them as reference particles. This can be circumvented by assessing polystyrene beads and cells relative each other instead of measuring absolute contrast factors. Since their contrast factor should be calculated under the same conditions and using the same reference particle, it is possible to calculate the ratio between their contrast factors and use this knowledge to tune the separation settings.

Furthermore, the findings that the polystyrene beads slightly differ can potentially be used to test and evaluate the current results by attempting to separate similarly sized but differently coloured polystyrene beads.

Another potential issue and room for future improvement might be the current lack of temperature monitoring within the set-up. Acoustic energy density is sensitive to fluctuations in fluid temperature and the piezotransducers might heat up due to prolonged usage. In the current set-up we counter this by waiting a few seconds between each measurement and the self-reference experiment should have indicated any changes over time. Actively monitoring the temperature might however be another step to further improve the experimental set-up.

Experiments with Melamine resin resulted in a contrast factor not quite the same as could be found in literature, but most definitely within a reasonable range of what

could be expected from a particle with its properties, being denser than polystyrene.

As the first experiments using cells were made certain issues arose. The cells did not give of enough auto-fluorescence to be imaged and tracked properly. Attempts to stain and consequently image cells failed, although comparisons with FACS showed that staining was successful.
This issue was resolved during the last stages of the thesis, as it was discovered that the optical cable between the light source and the microscope was damaged, loosing much of its efficiency. With a new cable, the cells became visible enough to track them and the preliminary results on the breast cancer cells indicate some good potential for separation.

Overall, this thesis resulted in a good step towards establishing a reliable and accurate experimental model that can measure the acoustic contrast factor of particles using a reference particle to determine the conditions of the acoustic field, i.e. the acoustic energy density. The model still requires a bit more evaluation and improvements, especially in regards to measuring cells, and many processes and steps could potentially be optimised in the future development to ensure the best possible tool for use in biomedical research.

6

Practical Applications and Future Outlook

As this thesis draws to a close, it is of great interest to consider future improvements, potential experiments that would further help in evaluating the model and how this model might be used in practical applications. Some of these points had already been touched upon when discussing the results of experiments within this thesis or within the conclusions, but it might be of interest to have a more concrete summary of those.

In terms of the computational model, following improvements and experiments might be of interest in future developments:

- The MatLab scripts could be simplified and made more intuitive to enable easier usage. An ambitious development of this might be the creation of a GUI script that enables simple input of parameters and data, automates the data processing and quickly gives numerical and graphical results.
- The model could be expanded to include the measurement of both particle density and compressibility instead of only the acoustic contrast factor. This can be done by measuring the same particle with different buffer solutions.
- A mathematical formula could be implemented to automate the selection of a reasonable velocity filter.
- The model could be expanded to focus more on the relative acoustic properties of particles instead of their absolute values, thus reducing the impact of potential inaccuracies of the reference particle.

The experimental set-up has the most room for improvement and experiments, such as:

- Tracking and measuring additional live cells and using the results to attempt cell separations from homogeneous solutions.

- Inclusion of temperature control, as this would give more information about the conditions in the set-up.
- Changing the design of the chip such that the migration is actuated by a piezo-transducer mounted on the side of the channel instead of below.
- Experiments involving various buffers with different acoustic properties and evaluation of their effect on the measurements.
- Final experiments in the development of this tool would be direct comparisons of separations using buffers calculated by this model with conventional separation methods and evaluation of the efficiency and purity of separation.

Assuming that future development continues in a positive direction, it should be possible to establish an easy and accurate method to measure the acoustic properties of particles and cells in a medium and make it possible to evaluate if, and how, a heterogeneous solution might best be separated. The experiment itself requires relatively few steps and can give results within a few hours, making it easier to separate cells by acoustophoresis and thus making the technique even more competitive compared to other separation methods.

7

Populärvetenskaplig Artikel

I många medicinska sammanhang är man intresserad av att kunna separera olika celltyper från varandra, exempelvis vita blodkroppar från ett blodprov eller insulinproducerande celler från bukspottskörteln. Det finns ett antal olika metoder för att genomföra denna separation. En tämligen ny metod bygger på akustofores, vilket betyder "att flytta med ljud."

För att förstå hur detta fungerar behöver vi först förstå vad ljud och ljudvågor är. Ljud uppstår då ett föremål vibrerar fram och tillbaka. Detta orsakar rörelse i dess omgivning, vare det sig är en gas, vätska eller ett fast föremål. Denna rörelse breder ut sig i en vågform från objektet. Tiden mellan två separata vågor beror på hur snabbt föremålet vibrerar och kallas för vågens frekvens. Stöter denna våg mot andra föremål kan den antingen reflekteras eller tas upp och fortsätter sin rörelse in i det nya objektet.
Skulle en ljudvåg reflekteras fram och tillbaka mellan två ytor kan det hända att de blir superponerade, dvs. överlagrade, vilket skapar en våg som ser ut att stå stilla. Denna stående våg har noder, där vågens rörelse är som minst, och bukar, där vågens rörelse är som störst.

Akoustoforesen bygger på principen att när ljudvågor träffar på en cell knuffar de på den. Hur mycket den flyttas beror på cellens akustiska mobilitet, vilket är en egenskap beroende på dess storlek, densitet och kompressibilitet (dvs. hur lätt det är för ett material att ändra sin form då det utsätts för en kraft) i förhållande till den omgivande vätskans egenskaper.

För att kunna separera celler på ett effektivt sätt med hjälp av ljudvågor behöver man ett sätt att mäta deras akustiska mobilitet. Att mäta deras storlek är relativt enkelt och det finns många väletablerade metoder för att göra det, men att mäta deras densitet och kompressibilitet är inte alls lika etablerat. I detta examensarbete har det utvecklats en metod för att göra just detta.
Metoden går ut på att fylla en mikrokanal, dvs. en kanal med dimensioner på mikrometerskalan, med en vätska som innehåller celler som man vill bestämma

egenskaperna av tillsammans med en referenspartikel med redan känd densitet och kompressibilitet, t.ex. mikrometer stora kulor gjorda av glas eller plast. Fördelen med mikrofluidiska kanaler är att vätskor och partiklar beter sig mer förutsägbart på små storleksskalor än på stora storleksskalor tack vare en effekt som kallas laminärt flöde. I laminärt flöde följer strömningen parallella linjer istället för att blandas. Detta gör laminärt flöde väldigt användbart i forskningsändamål där man vill kontrollera vätskors och partiklars rörelse.

Sedan skapas det ljudvågor i kanalen med hjälp av en ultraljudsgivare. Genom att använda en lämplig frekvens kan man skapa en stående våg med dess nod precis i mitten av kanalen. Då vågornas rörelse är som minst där kommer cellerna att börja röra sig mot mitten på grund av kollisionerna med vågorna. Medans cellerna och referenspartiklarna rör sig mot mitten tas det en bildserie. Med hjälp av denna bildserie kan man, i ett datorprogram, räkna ut hur snabbt cellerna och partiklarna rörde sig. Eftersom man vet den akustiska mobiliteten hos referenspartiklarna kan man använda den relativa hastigheten mellan cellerna och partiklarna för att räkna ut den akustiska mobiliteten hos cellerna också. Genom att återupprepa detta experiment under olika förhållanden, t.ex. med olika vätskor, kan man analysera hur den relativa hastigheten mellan cellen och partikeln ändras och även räkna ut cellens exakta densitet och mobilitet.
I det här arbetet utfördes det främst konfigering av den experimentella uppställningen samt optimering av datorprogrammet som används vid beräkningarna. För detta ändamål användes främst plastpartiklar i olika storlekar och egenskaper. Uppställningen visar lovande resultat och kan beräkna partiklarnas akustiska mobilitet med försumbara felmarginaler. Initialla tester med tre olika typer av bröstcancerceller visar tydliga skillnader i deras akustiska egenskapar, vilket som kan användas för att anpassa experimentella inställningar och lösningar för att optimera skillnaden i deras akustiska mobilitet, vilket skulle göra separation med hjälp av akustofores av de mycket mer effektiv.

Bibliography

[1] M. J. Tomlinson, S. Tomlinson, X. B. Yang, and J. Kirkham. *"Cell separation: terminology and practical considerations"*. Journal of tissue engineering 4 (2013), p. 2041731412472690.

[2] M. Onoe and H. Jumonji. *"Useful formulas for piezoelectric ceramic resonators and their application to measurement of parameters"*. The Journal of the Acoustical Society of America 41:4B (1967), pp. 974–980.

[3] E. S. Menon. *Transmission pipeline calculations and simulations manual*. Gulf Professional Publishing, 2014.

[4] Bruus, H. (2011)." *Acoustofluidics 1: Governing equations in microfluidics."* Lab on a Chip, 11(22), 3742-3751.

[5] H. Faxén. *"Der widerstand gegen die bewegung einer starren kugel in einer zähen flüssigkeit, die zwischen zwei parallelen ebenen wänden eingeschlossen ist"*. Annalen der Physik 373:10 (1922), pp. 89–119.

[6] J. Friend and L. Y. Yeo. *"Microscale acoustofluidics: microfluidics driven via acoustics and ultrasonics"*. Reviews of Modern Physics 83:2 (2011), p. 647.

[7] M. Gedge and M. Hill. *"Acoustofluidics 17: theory and applications of surface acoustic wave devices for particle manipulation"*. Lab on a Chip 12:17 (2012), pp. 2998–3007.

[8] K. Yosioka and Y. Kawasima. *"Acoustic radiation pressure on a compressible sphere"*. Acta Acustica united with Acustica 5:3 (1955), pp. 167–173.

[9] M. Settnes and H. Bruus. *"Forces acting on a small particle in an acoustical field in a viscous fluid"*. Physical Review E 85:1 (2012), p. 016327.

[10] T. M. Squires and S. R. Quake. *"Microfluidics: fluid physics at the nanoliter scale"*. Reviews of modern physics 77:3 (2005), p. 977.

[11] H. Schlichting and K. Gersten. *Boundary-layer theory*. Springer Science & Business Media, 2003.

[12] S. Boluriaan and P. J. Morris. *"Acoustic streaming: from Rayleigh to today"*. International Journal of aeroacoustics 2:3 (2003), pp. 255–292.

[13] H. Bruus. *"Acoustofluidics 7: the acoustic radiation force on small particles"*. Lab on a Chip 12:6 (2012), pp. 1014–1021.

[14] M. W. Ley and H. Bruus. *"Continuum modeling of hydrodynamic particle–particle interactions in microfluidic high-concentration suspensions"*. Lab on a Chip 16:7 (2016), pp. 1178–1188.

[15] Baasch, T., Reichert, P., Lakämper, S., Vertti-Quintero, N., Hack, G., i Solvas, X. C., ... & Dual, J. (2018). *"Acoustic compressibility of Caenorhabditis elegans."* Biophysical journal, 115(9), 1817-1825.

[16] Bruus, H. (2012). *"Acoustofluidics 10: scaling laws in acoustophoresis."* Lab on a Chip, 12(9), 1578-1586.

[17] M. Barmatz and P. Collas. *"Acoustic radiation potential on a sphere in plane, cylindrical, and spherical standing wave fields"*. The Journal of the Acoustical Society of America 77:3 (1985), pp. 928–945.

[18] J. Hurley. *"Sizing particles with a coulter counter"*. Biophysical journal 10:1 (1970), pp. 74–79.

[19] W. M. Haynes, D. R. Lide, and T. J. Bruno. *CRC handbook of chemistry and physics*. CRC press, 2016.

[20] L. D. Landau, E. M. Lifshitz, A. M. Kosevich, and L. P. Pitaevskii. *Theory of elasticity: volume 7*. Vol. 7. Elsevier, 1986.

[21] P. H. Mott, J. R. Dorgan, and C. Roland. *"The bulk modulus and poisson's ratio of "incompressible" materials"*. Journal of Sound and Vibration 312:4-5 (2008), pp. 572–575.

[22] P. Ewald. *"Der ultraschall und seine anwendung in wissenschaft und technik by l. bergmann"*. Acta Crystallographica 8:1 (1955), pp. 69–70.

[23] Hartono, D., Liu, Y., Tan, P. L., Then, X. Y. S., Yung, L. Y. L., & Lim, K. M. (2011). *"On-chip measurements of cell compressibility via acoustic radiation."* Lab on a Chip, 11(23), 4072-4080.

[24] Barnkob, R., Augustsson, P., Laurell, T., & Bruus, H. (2010). *"Measuring the local pressure amplitude in microchannel acoustophoresis."* Lab on a Chip, 10(5), 563-570.

[25] Barnkob, R., Augustsson, P., Laurell, T., & Bruus, H. (2012). *"Acoustic radiation-and streaming-induced microparticle velocities determined by microParticle Tracking Velocimetry in an ultrasound symmetry plane."* Physical Review E, 86(5), 056307.

[26] R. Barnkob, C. J. Kähler, and M. Rossi. *"General defocusing particle tracking"*. Lab on a Chip 15:17 (2015), pp. 3556–3560.

[27] Cushing, K. W., Garofalo, F., Magnusson, C., Ekblad, L., Bruus, H., & Laurell, T. (2017). *"Ultrasound characterization of microbead and cell suspensions by speed of sound measurements of neutrally buoyant samples"*. Analytical chemistry, 89(17), 8917-8923.

[28] Lasfargues, E. Y., & Ozzello, L. (1958). *"Cultivation of human breast carcinomas"*. Journal of the National Cancer Institute, 21(6), 1131-1147.

[29] Neve, R. M., Chin, K., Fridlyand, J., Yeh, J., Baehner, F. L., Fevr, T., ... & Gray, J. W. (2006). *"A collection of breast cancer cell lines for the study of functionally distinct cancer subtypes"*. Cancer cell, 10(6), 515-527.

[30] Soule, H. D., Vazquez, J., Long, A., Albert, S., & Brennan, M. (1973). *"A human cell line from a pleural effusion derived from a breast carcinoma"*. Journal of the national cancer institute, 51(5), 1409-1416.

8

Appendix

8.1 A: Mobility and Contrast Ratios

Tables with the acoustic mobility ratio and contrast factor ratio in both the PTV set-up and the position difference set-up.

Table 8.1 Mobility ratio

	Lateral displacement		PTV	
	Average	90% Confidence	Average	90% Confidence
Red (4.99)/Green (7.81)	0,473	0,469-0,481	0,523	0,510-0,539
Green(5.18)/Red (9.89)	0,337	0,326-0,348	0,343	0,335-0,342
Green (5.18)/Green(7.81)	0,462	0,449-0,476	0,479	0,466-0,493
Red(4.99)/Red(9.89)	0,306	0,300-0,312	0,371	0,364-0,379
Melamine (5)/Red(9.89)	0,580	0,569-0,591	0,449	0,434-0,467

Table 8.2 Contrast factor

	Lateral displacement		PTV	
	Average	90% Confidence	Average	90% Confidence
Red (4.99)/Green (7.81)	1,16	1,15-1,18	1,28	1,25-1,32
Green(5.18)/Red (9.89)	1,23	1,18-1,27	1,25	1,21-1,28
Green (5.18)/Green(7.81)	1,05	1,02-1,08	1,09	1,06-1,12
Red(4.99)/Red(9.89)	1,20	1,18-1,23	1,46	1,43-1,49
Melamine (5)/Red(9.89)	2,27	2,23-2,31	1,76	1,70-1,83

8.2 B: Contrast factor Cells

The contrast factor of three different types of breast cancer cells were measured with our set-up

Table 8.3 The field of view was sequenced into 12 adjacent slices, each 50 μm wide. Using 5.00 μm Red PS beads as reference particles to calculate the energy density at the various slices of the field of view, the energy density was subsequently used to calculate the contrast factor of three BT-20 cell samples. All samples were measured at the same position along the chip, with a levitation frequency of 4.89 MHz and a migration frequency of 1.96 MHz. The peak to peak voltages in the piezotransducers were kept at 1.27 V_{pp} for the levitation and 1.3 V_{pp} for the migration. The particle concentration was $0.3 \cdot 10^6$ Particles/ml for the reference particles and $0.2 \cdot 10^6$ cells/ml for the BT-20 cells, each suspended in PBS.

	Φ Reference	E_{ac} (Pa)	Φ Sample 1	Φ Sample 2	Φ Sample 3
Slice 1	0.141	16.50	0.003	0.005	0.002
Slice 2	0.141	16.55	0.005	0.004	0.008
Slice 3	0.141	15.65	0.004	0.005	0.004
Slice 4	0.141	14.59	0.005	0.005	0.003
Slice 5	0.141	15.41	0.004	0.003	0.009
Slice 6	0.141	14.70	0.004	0.004	0.008
Slice 7	0.141	14.88	0.005	0.003	0.005
Slice 8	0.141	13.90	0.003	0.005	0.005
Slice 9	0.141	14.50	0.005	0.003	0.004
Slice 10	0.141	14.80	0.004	0.004	0.005
Slice 11	0.141	14.70	0.004	0.003	0.005
Slice 12	0.141	14.86	0.003	0.004	0.006
Φ_{mean}	0.004				
SD	0.001				

Table 8.4 The field of view was sequenced into 12 adjacent slices, each 50 μm wide. Using 5.00 μm Red PS beads as reference particles to calculate the energy density at the various slices of the field of view, the energy density was subsequently used to calculate the contrast factor of three BT-549 cell samples. All samples were measured at the same position along the chip, with a levitation frequency of 4.89 MHz and a migration frequency of 1.96 MHz. The peak to peak voltages in the piezotransducers were kept at 1.27 V_{pp} for the levitation and 1.3 V_{pp} for the migration. The particle concentration was $0.3 \cdot 10^6$ Particles/ml for the reference particles and $0.2 \cdot 10^6$ cells/ml for the BT-549 cells, each suspended in PBS.

	Φ Reference	E_{ac} (Pa)	Φ Sample 1	Φ Sample 2	Φ Sample 3
Slice 1	0.141	18.86	0.004	0.012	0.010
Slice 2	0.141	19.07	0.007	0.011	0.008
Slice 3	0.141	19.23	0.004	0.007	0.010
Slice 4	0.141	18.18	0.006	0.010	0.008
Slice 5	0.141	18.57	0.010	0.010	0.007
Slice 6	0.141	15.37	0.008	0.008	0.008
Slice 7	0.141	18.82	0.007	0.006	0.008
Slice 8	0.141	16.30	0.009	0.011	0.010
Slice 9	0.141	15.95	0.006	0.010	0.010
Slice 10	0.141	16.58	0.004	0.011	0.009
Slice 11	0.141	18.00	0.006	0.009	0.008
Slice 12	0.141	17.22	0.007	0.009	0.010
Φ_{mean}	0.009				
SD	0.003				

Table 8.5 The field of view was sequenced into 12 adjacent slices, each 50 μm wide. Using 5.00 μm Red PS beads as reference particles to calculate the energy density at the various slices of the field of view, the energy density was subsequently used to calculate the contrast factor of three MCF-7 cell samples. All samples were measured at the same position along the chip, with a levitation frequency of 4.89 MHz and a migration frequency of 1.96 MHz. The peak to peak voltages in the piezotransducers were kept at 1.27 V_{pp} for the levitation and 1.3 V_{pp} for the migration. The particle concentration was $0.3 \cdot 10^6$ Particles/ml for the reference particles and $0.2 \cdot 10^6$ cells/ml for the MCF-7 cells, each suspended in PBS.

	Φ Reference	E_{ac} (Pa)	Φ Sample 1	Φ Sample 2	Φ Sample 3
Slice 1	0.141	11.99	0.008	0.011	0.007
Slice 2	0.141	12.26	0.008	0.009	0.017
Slice 3	0.141	13.40	0.008	0.007	0.013
Slice 4	0.141	14.68	0.009	0.006	0.014
Slice 5	0.141	7.31	0.014	0.012	0.015
Slice 6	0.141	11.29	0.009	0.007	0.010
Slice 7	0.141	11.84	0.011	0.009	0.012
Slice 8	0.141	12.62	0.011	0.009	0.010
Slice 9	0.141	11.69	0.008	0.009	0.012
Slice 10	0.141	11.26	0.011	0.009	0.009
Slice 11	0.141	12.81	0.006	0.009	0.011
Slice 12	0.141	11.92	0.007	0.008	0.012
Φ_{mean}	0.010				
SD	0.003				